AGU PUBLICATIONS

JGR

Journal of Geophysical Research: Oceans

RESEARCH ARTICLE

10.1002/2016JC012554

An idealized study of near equatorial river plumes

Elbio D. Palma[1] and Ricardo P. Matano[2]

[1]Departamento de Física, Universidad Nacional del Sur, and Instituto Argentino de Oceanografía, Bahia Blanca, Argentina, [2]College of Earth, Oceanic and Atmospheric Sciences, Oregon State University, Corvallis, Oregon, USA

Key Points:
- Near equatorial river plumes can be characterized as beta-plumes
- Eddy merging arrests the decay of the plume against mixing effects
- Freshwater discharges on stratified basins generate cyclones that pump saltier water to the surface thus eroding the low-salinity signal

Correspondence to:
E. D. Palma,
uspalma@criba.edu.ar

Citation:
Palma, E. D., and R. P. Matano (2017), An idealized study of near equatorial river plumes, *J. Geophys. Res. Oceans*, *122*, doi:10.1002/2016JC012554.

Received 18 NOV 2016
Accepted 25 MAR 2017
Accepted article online 31 MAR 2017

Abstract The dynamics of near equatorial river plumes (NERPs) are investigated using a highly idealized model. The spreading of a NERP from an eastern boundary is characterized by a continuous shedding of westward propagating eddies. This process transfers the bulk of the freshwater discharge to the deep ocean, thus distinguishing NERPs from their midlatitude counterparts. In the long-term limit, a NERP can be rationalized as a β-plume emanating from a coastal source. The evolution of NERPs in an unstratified basin is quite different from that in a stratified one. The spin-up in an unstratified basin is characterized by the formation of an anticyclonic bulge, which spreads westward thus creating a density stratification that favors the subsequent development of smaller and faster moving secondary eddies. The collision of the secondary eddies with the leading bulge arrests the effects of mixing thus allowing the further spreading of the buoyancy anomaly. In a stratified basin, the generation of anticyclonic eddies is accompanied by a concurrent generation of cyclones, which pump saltier waters to the surface hence leading to smaller sea surface salinity (SSS) anomalies. NERPs are sensitive to variations of the freshwater flux (Q_{fw}) and the geomorphological setting. Larger Q_{fw} generates bigger eddies, which spread at a rate proportional to the square root of the normalized flux. Wide shelves allow the interaction of the eddies with the bottom, thus promoting a cyclonic shift of the axis of the eddy train. The inclination of the coast affects the dynamical balance controlling the near-field behavior of NERPs.

1. Introduction

The Congo River is the inspiration of this article. It discharges an average of 40,000 m^3/s of freshwater into the deep ocean, making it the second largest river in the world [*Dai et al*., 2009]. This freshwater input has a profound impact on the physical and biogeochemical properties of the eastern tropical Atlantic. The Congo plume can be traced for more than 1000 km offshore [*Hopskins et al*., 2013; *Chao et al*., 2015], thus affecting the freshwater balance, density stratification, and concentration of nutrients, carbon, and contaminants of a vast portion of the eastern Atlantic equatorial region. The magnitude of the salinity anomaly flux generated by the Congo River discharge is of the same order than the salinity anomaly flux produced by the Mediterranean outflow in the eastern North Atlantic (although of different sign), and its annual freshwater input to the tropical Atlantic is comparable to that of the annual mean precipitation by the ITCZ. The Congo freshwater discharge also increases the stratification of the tropical waters thus inhibiting vertical mixing and influencing the sea surface temperatures [*Materia et al*., 2012].

Theory predicts, and observations confirm, that near equatorial freshwater discharges, such as those of the Congo River, generate surface-advected plumes, which are confined to the upper layers of the ocean and, therefore, not significantly affected by the bottom topography [*Yankovsky and Chapman*, 1997; *Chao et al*., 2015]. At midlatitudes, surface-advected plumes are characterized by the formation of a bulge at the mouth of the estuary and a coastal current [*Garvine*, 1999; *Yankovsky*, 2000; *Fong and Geyer*, 2002; *García Berdeal et al*., 2002]. The size of the bulge and the transport of the coastal current depend on the inlet Rossby number $R_{oi} = uf/W$, where u is the outflow velocity, f the Coriolis parameter, and W the width of the inlet [*Fong and Geyer*, 2002]. For large outflows, the bulge retains more than 65% of the discharge while the remains are funneled to a narrow coastal current flowing in the Kelvin wave direction [*Nof and Pichevin*, 2001; *Fong and Geyer*, 2002]. The time evolution of the bulge and the coastal plume depend on the geographical location of the outflow. On a midlatitude f-plane, the growth of the bulge is limited by the development of baroclinic instabilities [*Oey and Mellor*, 1993], which lead to the eventual disappearance of the bulge structure

[*Vic et al*., 2014]. For outflows located in low latitudes, the dynamics is controlled by the meridional gradient of the Coriolis parameter (β) and the long-term evolution of the system depends critically on the orientation of the wall where the outflow occurs [*Nof et al*., 2004]. The Congo River outflow is located at a few degrees off the equator on the eastern Atlantic coast and therefore theory anticipates the detachment and westward migration of the bulge formed during the spin-up process [*Nof et al*., 2002].

There are very few studies on the dynamics of NERPs. One of the most important, albeit not originally focused on NERPs, is that of *Nof et al*. [2002, hereinafter NPS02], who predicted that a low-latitude buoyant outflow from an eastern boundary should generate a train of westward moving anticyclonic eddies. They also predicted that the bulk of the freshwater should be diverted to the coastal current. In a later modeling study of the Congo River plume, *Denamiel et al*. [2013] argued that, in the absence of wind forcing, the plume should follow the coastline toward the northwest. They ascribed this result, which is in conflict with NPS02 arguments, to the influence of the geomorphology on the plume dynamics. More recently, *Vic et al*. [2014, hereinafter VIC14] analyzed numerical simulations of the Congo plume in a highly idealized setup. Their simulation produced a highly irregular eddy field characterized by a leading eddy of large size instead of the train of regularly spaced and noninteracting eddies described by NPS02.

The NPS02 and VIC14 studies highlight the contribution of the β-dynamics on NERPs. Here we show that eddy-to-eddy interaction is an important mechanism for the spreading of a NERP and the reestratification of the basin. Through scaling arguments, we also show that in the long-term asymptotic limit, a NERP can be rationalized as a β-plume emanating from a coastal source. Our experiments show that—in disagreement with the analytical predictions of NPS02—the bulk of the freshwater discharge is not trapped in the nearshore region but it is transported offshore by eddies. Finally, we show that the spreading rate and salinity structure of NERPs are modulated by the magnitude of the freshwater flux, the geographical location of the outflow, the inclination of the coast, the depth of the shelf, and the background stratification.

2. Model Description

The numerical model used in this study is the Regional Ocean Model System (ROMS) [*Shchepetkin and McWilliams*, 2005]. The model domain is set in a southern hemisphere β-plane and consists of a rectangular basin centered near 6°S that is 12° long (*y* direction) and 28° wide (*x* direction), with a horizontal grid resolution of 1/12 of a degree and 30 s levels in the vertical. The ocean is initially quiescent and it has a constant reference density computed with a fixed temperature (20°C) and salinity (35 psu). The southern, northern, and western sides of the domain are open boundaries, there we impose the Flather radiation condition on the barotropic variables (depth-averaged velocities and sea surface elevation) and the Orlanski radiation condition on the baroclinic velocities and tracers [*Marchesiello et al*., 2001]. At the western boundary, there is a 100 km wide sponge layer with increased horizontal viscosity coefficient. Table 1 list all the experiments

Table 1. Characteristics of the Numerical Experiments Described in the Text

Experiment	Initial Stratification	Q (m^3/s)	ΔS	Location	Topography (m)	Coastline	Obs
BENCH	S = 35	40,000	15.0	6°S, 13.5°E	H = 1000	Meridional	
BSTOP1	S = 35	40,000	15.0	6°S, 13.5°E	H = 1000	Meridional	Variable Q
BSTOP2	S = 35	40,000	15.0	6°S, 13.5°E	H = 1000	Meridional	Variable Q
BBART	S = 35	40,000	0	6°S, 13.5°E	H = 1000	Meridional	
HDLS	S = 35	160,000	3.75	6°S, 13.5°E	H = 1000	Meridional	
LDHS	S = 35	20,000	30.0	6°S, 13.5°E	H = 1000	Meridional	
LQFW	S = 35	10,000	15.0	6°S, 13.5°E	H = 1000	Meridional	
HQFW	S = 35	160,000	15.0	6°S, 13.5°E	H = 1000	Meridional	
LAT3E	S = 35	40,000	15.0	3°S, 13.5°E	H = 1000	Meridional	
LAT6W	S = 35	40,000	15.0	6°S, 10°W	H = 1000	Meridional	
SHELFN	S = 35	40,000	15.0	6°S, 13.5°E	Narrow shelf	Meridional	Bottom slope = 2.6×10^{-3}
SHELFW	S = 35	40,000	15.0	6°S, 13.5°E	Wide shelf	Meridional	Bottom slope = 4.25×10^{-4}
HCONST	S = 35	40,000	15.0	6°S, 13.5°E	H = 50	Meridional	
SLNE	S = 35	40,000	15.0	6°S, 13.5°E	H = 1000	Slanted NE	
SLNW	S = 35	40,000	15.0	6°S, 13.5°E	H = 1000	Slanted NW	
STRAT	N(z)	40,000	15.0	6°S, 13.5°E	H = 1000	Meridional	

to be discussed herein. In the benchmark case (BENCH), the bottom topography is set to a constant value $H = 1000$ m. At the eastern wall, there is an inlet, where we impose a fixed volume discharge $Q = 40{,}000$ m^3/s, which is close to the Congo River discharge, and a salinity of 20 psu (salinity anomaly 15 psu). The upstream edge of the inlet is located at 6°S, and it has width $W = 20$ km and depth $h_i = 30$ m (Figure 1a). The coefficients of vertical eddy viscosity K_M and diffusivity K_H are computed with the Mellor-Yamada closure scheme. A recursive MPDATA advection scheme is used for the tracer fields [*Smolarkiewicz and Grabowski*, 1990].

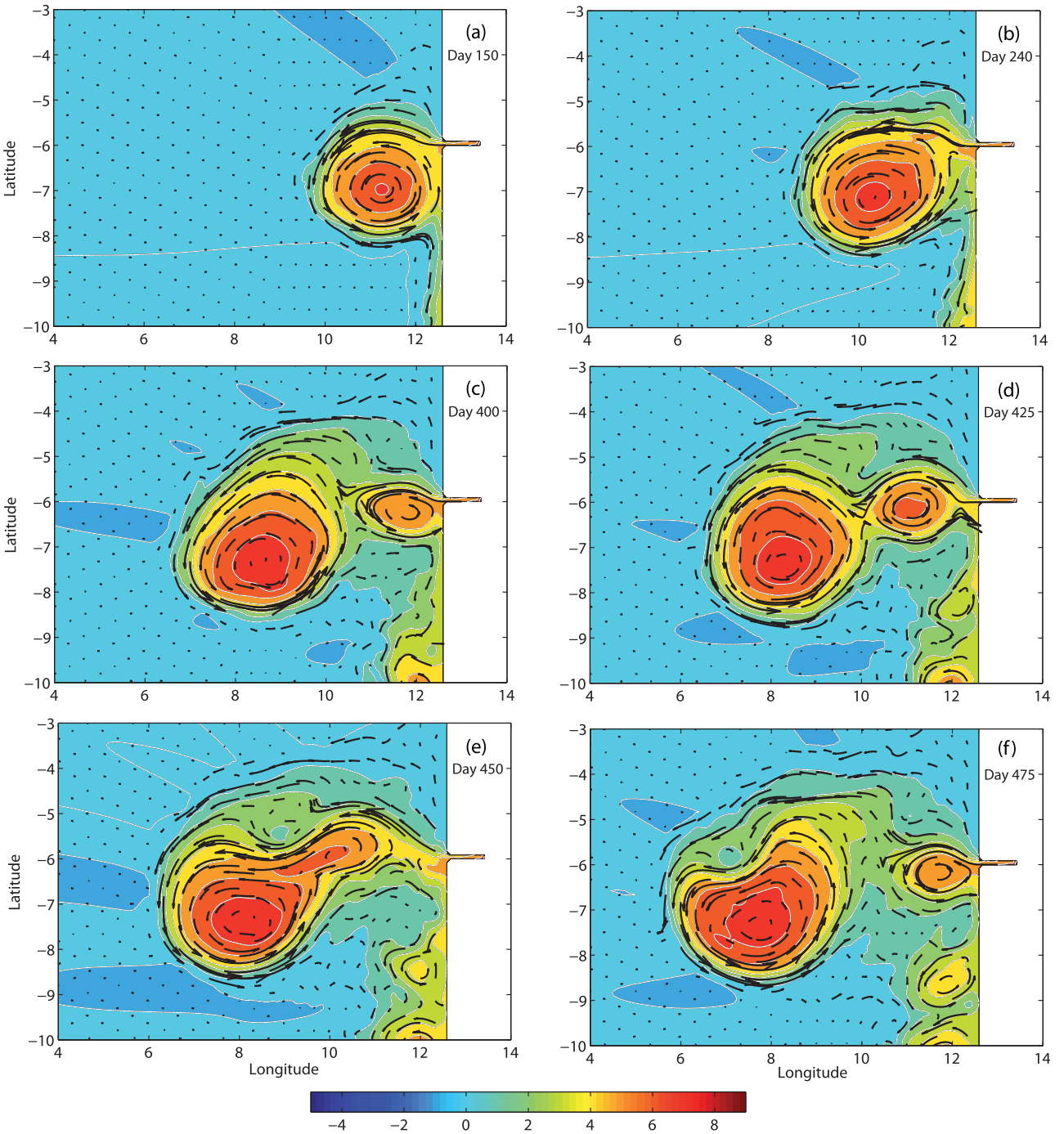

Figure 1. Snapshots of sea surface elevation and surface velocity vectors for the BENCH experiment showing the merging of anticyclonic eddies. Contour interval (CI = 2 cm).

3. Results

3.1. The Spin-Up

The spin-up of BENCH is illustrated with a sequence of SSH (sea surface elevation) and surface velocity vectors snapshots (Figure 1). At day 150, the plume resembles midlatitudes, *f*-plane depictions [e.g., *Yankovsky and Chapman*, 1997; *Fong and Geyer*, 2002], which are characterized by the formation of an anticyclonic bulge at the mouth of the estuary and a poleward flowing current along the continental boundary (Figure 1a). At day 240, however, the β-dynamics forces the detachment of the bulge from the coast and the formation of a large anticyclonic eddy (radius of ∼135 km) (Figure 1b). The westward migration of this eddy enables the development of a new bulge at the estuary's mouth (day 400, Figure 1c). This bulge, however, is not identical to the first on account of the fact that it develops in the stratified, moving medium created by the first bulge. The second eddy, therefore, migrates faster thus colliding and merging with the first one (Figures 1d and 1e). Subsequent eddy detachments lead to anticyclones of similar size (Figure 1f). The first eddy, which forms and moves in a quiescent, unstratified media, is substantially larger and slower than the trailing ones, which keep colliding and merging with it. These collisions and mergings are a regeneration process that arrests the decay of the first eddy. The importance of the first eddy on the spin-up process is clearly reflected in the time evolution of the basin averaged kinetic energy, which increases steadily during the first 6 years of the numerical simulation and drops abruptly after it leaves the model domain (Figure 2a). The exit of the first eddy from the domain leaves the basin filled with a westward train of smaller and faster anticyclonic eddies (Figure 3a). In the long-term average, the eddy-dominated propagation of the freshwater discharge manifests as a low-salinity plume that extends more than 1300 km westward form the river mouth (Figure 3b).

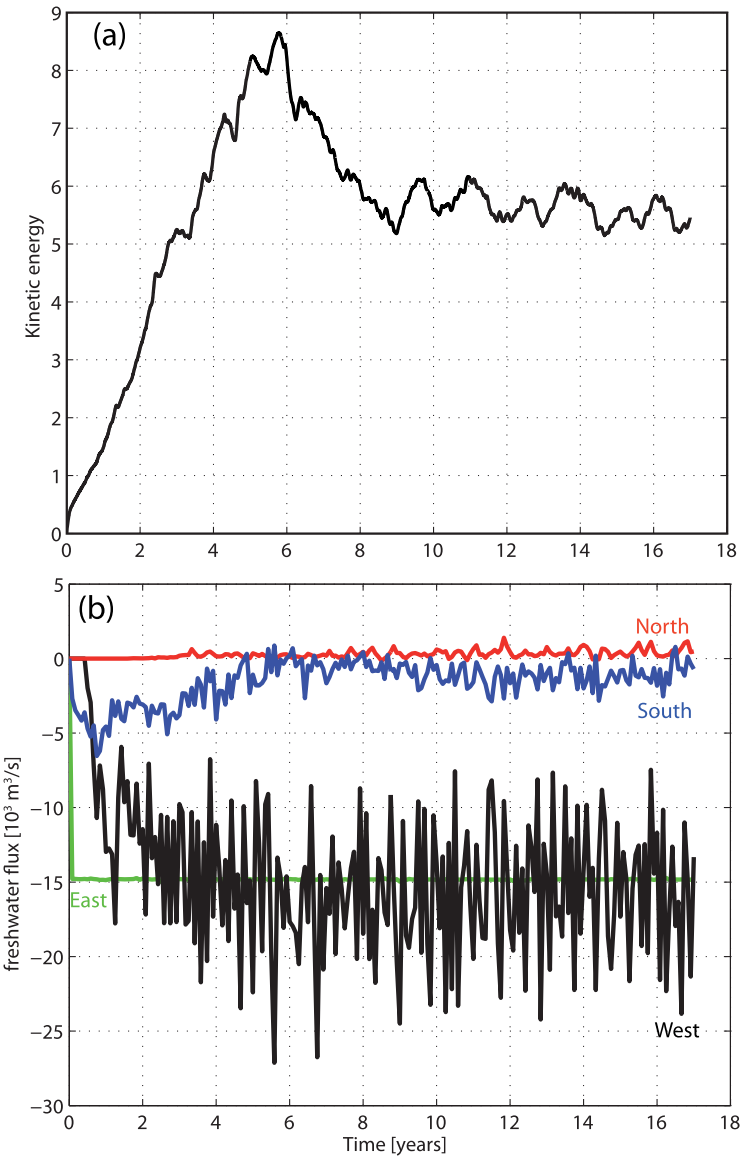

Figure 2. (a) Time evolution of the basin-averaged kinetic energy (J m^{-2}) for BENCH. (b) Time evolution of the freshwater transport through the walls of the box indicated in Figure 3a.

NPS02 predicted the eddy detachment observed in our simulation but did not anticipate the eddy collision process described above. As we shall see, eddy merging is a distinctive phase of the spin-up of an *unstratified*, near equatorial ocean that arrests the effects of mixing and generates the background density stratification that characterizes the buoyant plume.

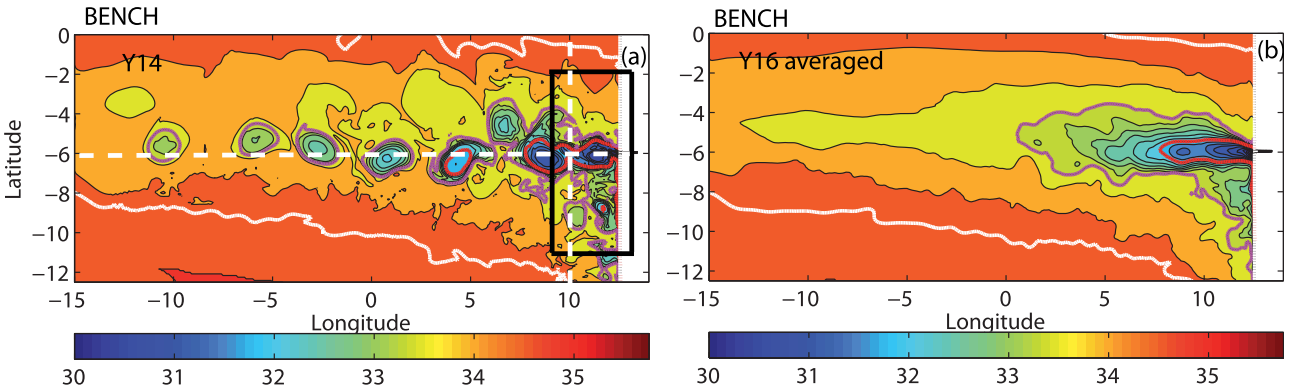

Figure 3. Sea surface salinity from the BENCH experiment: (a) snapshot at the end of year 14 of the simulation and (b) time-averaged result of the last year of simulation. CI = 0.25 until 33.5 and 0.5 until 35. The red, magenta, and white lines indicates the 32, 33.5, and 34.25 isohalines, respectively. The white dashed lines in Figure 3a indicate selected zonal and meridional cross sections discussed in the text. The black box indicates the control volume where the freshwater fluxes are computed.

3.2. Eddy Kinematics

We use SSH Hövmöller diagrams to characterize the properties of NERP eddies, namely: radius, detachment frequency, direction, and propagation speed (Figure 4). Following VIC14, we define the detachment period of the first eddy as the time taken for the eddy to cross the 10°E meridional cross section. Eddy merging, however, difficults the identification of the detachment period for the trailing eddies. In those cases, therefore, we define the detachment period as the average value of the time interval between zero crossings of the mean SSH (∼4.9 cm) at 10°E, 6°S (white line, Figures 4a and 4b). Eddy size is defined as the latitudinal extent of the 4.9 cm isoline at the instant when the eddy center crosses 10°E (Figure 4c). The first eddy has a detachment period T_{ed} = 240 days and a radius R_{ed} = 135 km. The secondary (trailing) eddies are smaller R_{ed} = 65 km and have a shorter detachment period T_{ed} = 32.5 days. The radius of the first eddy is in reasonable agreement with NPS02 analytical estimates, who—for the BENCH parameters—predicts a R_{ed} ∼ 120 km. The detachment period in the numerical simulations, however, is nearly half the analytical value. A similar discrepancy between simulations and theory was observed by NPS02 and VIC14.

At 6°S—the middle of the eddy corridor (Figure 3a)—there are two clearly defined propagation speeds (Figure 4d): 1.35 km/d (red line), which corresponds with the first eddy and 3.41 km/d (white lines), which corresponds with the trailing eddies. The NPS02 estimate of the propagation speed is

$$C = \frac{2}{3}\beta R_d^2 (2-\alpha)^{-1}, \tag{1}$$

where β is the gradient of the Coriolis parameter, R_d the Rossby radius of deformation, and $\alpha = 2v_\theta/r_o f_o$ a nondimensional parameter that represents nonlinear effects, with v_θ the eddy's azimuthal velocity, r_o the eddy radius, and f_o the Coriolis parameter. For the smaller eddies, $\alpha \sim 1.0$ (nonlinear regime) and $C \sim 3.26$ km/d. The analytical estimate, therefore, is substantially larger than the propagation speed of the first eddy in the numerical experiment but close to the value of the secondary eddies. As we shall show the difference between theoretical and numerical values is due to the fact that the first eddy moves into an unstratified environment while the secondary eddies move in the stratified medium created by the first eddy. NPS02 values are derived from a reduced-gravity model, which assumes a stratified medium.

3.3. The Vertical Structure of NERPs

Following *Garvine* [1999], we define the boundary of the buoyant plume as the 34.25 isohaline, which roughly corresponds with the 5% density anomaly. At day 240—when the first eddy detaches from the coast—the vertical penetration of the plume is of ∼30 m (Figure 5a, white line). By day 475, the merging of the first and the second eddy has deepened the plume by ∼5 m (Figure 5b). The trailing eddies have a minor penetration depth (∼20 m) on account of their smaller size. After the first eddy leaves the domain, the depth of penetration of the plume stabilizes at ∼30 m (Figure 5c). The time-averaged penetration depth at the end of the simulation is ∼25m at 0° (longitude) and it outcrops near 8°E (Figure 5d). At this stage, the average structure of the NERP resembles a β-plume, with surfacing of isopycnals in the upper layers and

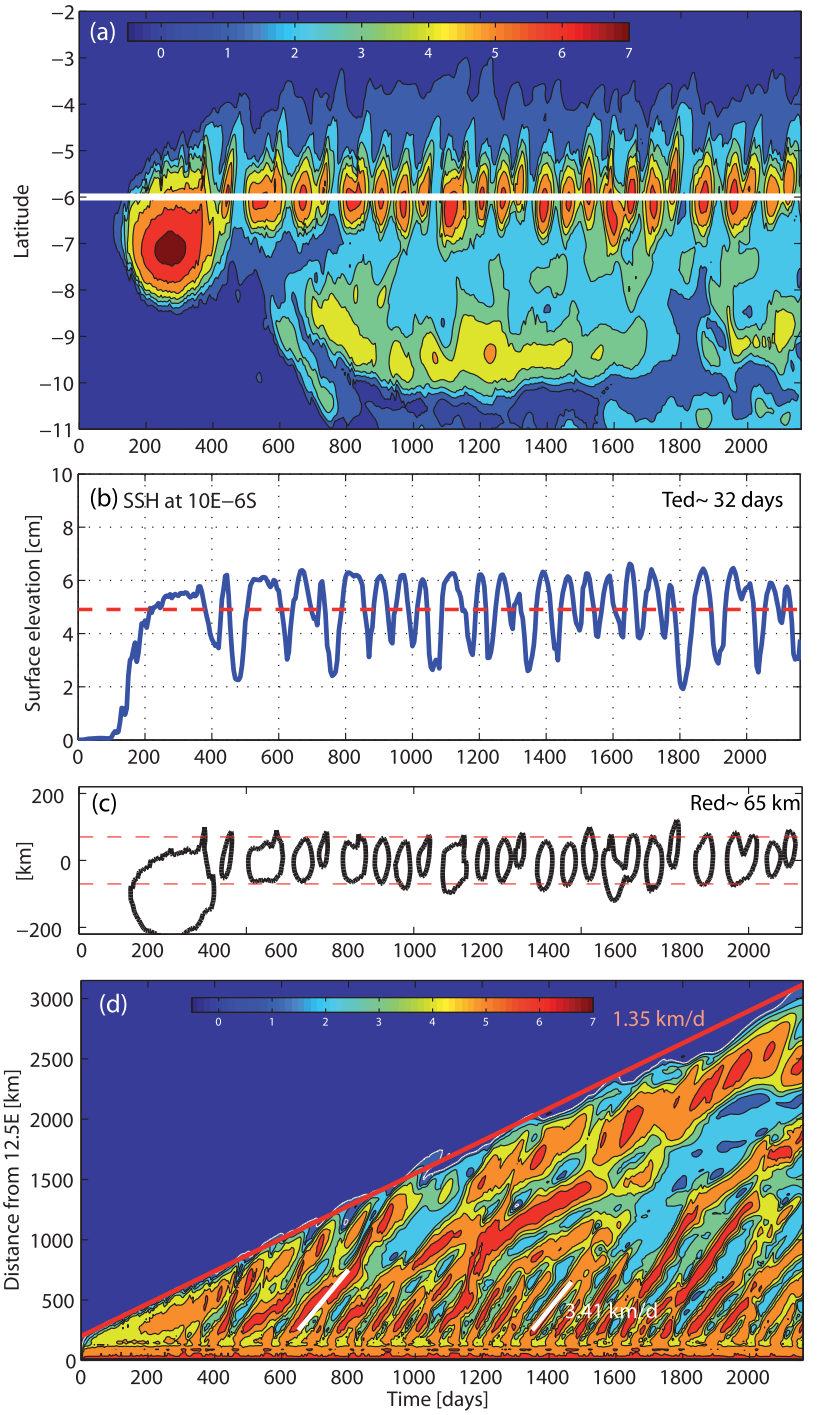

Figure 4. Eddy kinematics. (a) Hovmöller diagram of SSH at 10°E from the BENCH experiment. (b) Time evolution of SSH at 10°E, 6°S. The red dashed line indicates the mean value (4.9 cm). (c) Contours of the 4.9 cm isoline. (d) Hovmöller diagram of SSH at 6°S (white line in Figure 4a). The red line indicates the propagation speed of the first eddy, the white line is the approximate speed of the trailing eddies.

deepening at depth. The deepening has been ascribed to the downward propagation of the gravest baroclinic Rossby wave modes [*Beldamani et al.*, 2013].

3.4. Eddy Merging Effects

Eddy merging is an important mechanism for the spreading of a NERP in an unstratified basin; without it, the eddies would be constantly eroded by Rossby wave radiation and mixing [*Chassignet and Cushman-*

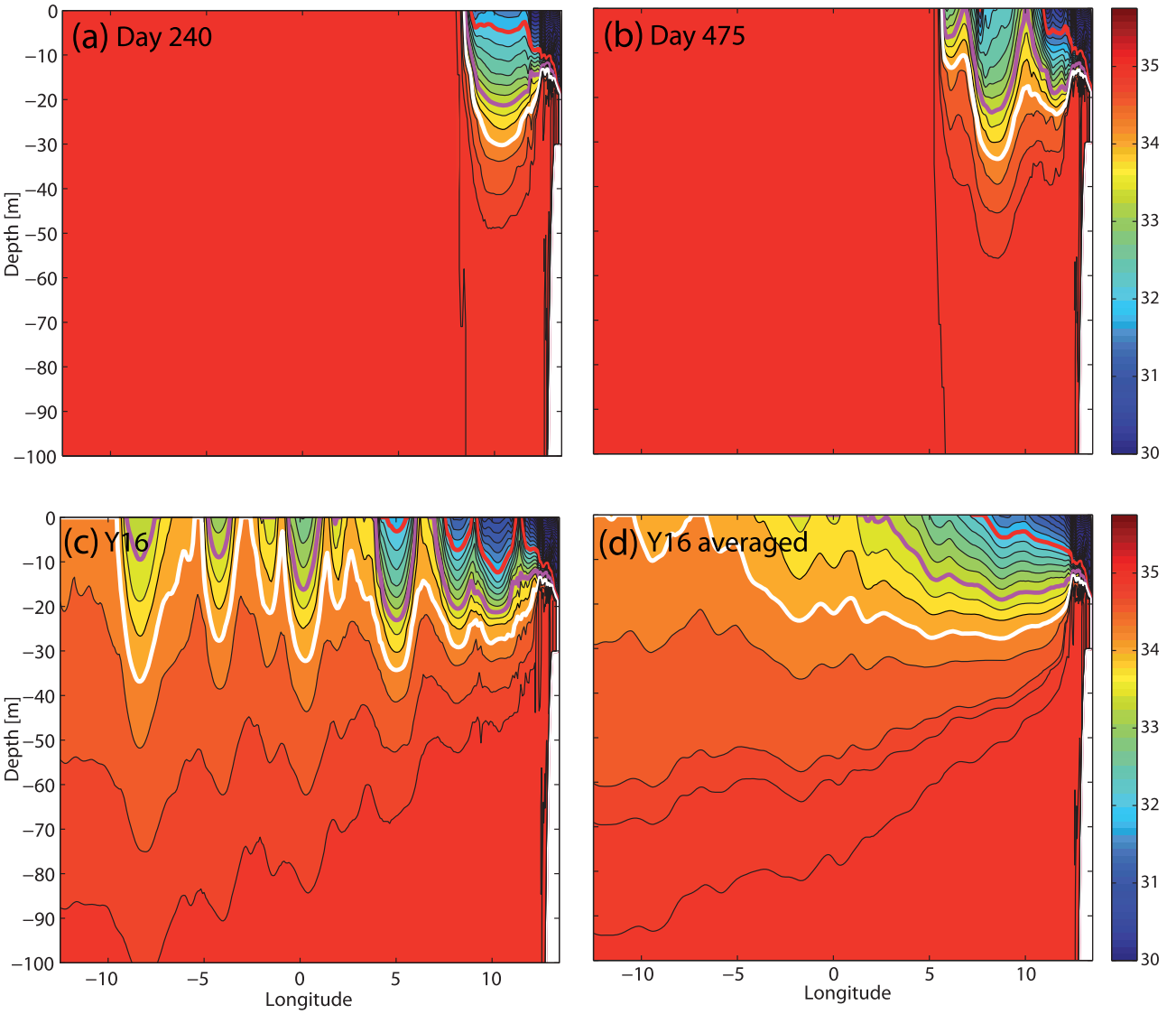

Figure 5. Salinity cross sections at 6°S from the BENCH experiment. (a–c) Snapshots and (d) the time-average of the last year of integration. CI = 0.25 until 34.75 and 0.1 thereafter. The red, magenta, and white lines indicates the 32, 33.5, and 34.25 isohalines, respectively.

Roisin, 1991]. To illustrate these matters, we did two additional experiments using a setup similar to BENCH but varying the duration of the river discharge. BSTOP1 shows the effects of wave radiation and mixing on an isolated eddy. In this experiment, the river discharge is shut off at the time of detachment of the first bulge, thus leaving a large eddy near the mouth of the river (the original bulge) and a smaller eddy farther south, which emerges from the remnants of the coastal current (Figure 6a). Their westward propagation is characterized by a relatively rapid decay and a small poleward tilt of their path. Similar features have been reported in studies of isolated lenses [*Chassignet and Cushman-Roisin*, 1991]. Thus, lack of eddy merging leads to the decay of the first eddy thus reducing the spreading rate of the plume; in BENCH, it is nearly constant but in BSTOP1 it changes with time (Figure 6b). These variations are partly associated with the small meridional migrations of the eddy but mostly with its decay [equation (1)]. The time-average plume of BSTOP1 shows substantial shrinking of the plume in the horizontal and the vertical (Figures 7a and 7b).

Eddy merging is a continuous process in BENCH, particularly during the initial phase of the experiment when secondary eddies interact with the leading one just after its detachment from the wall (Figure 1). The experiment BSTOP2 was designed to characterize the impact of eddy merging on the plume evolution in a more controlled sequence. To achieve this, we control the rate of eddy formation by turning on/off the

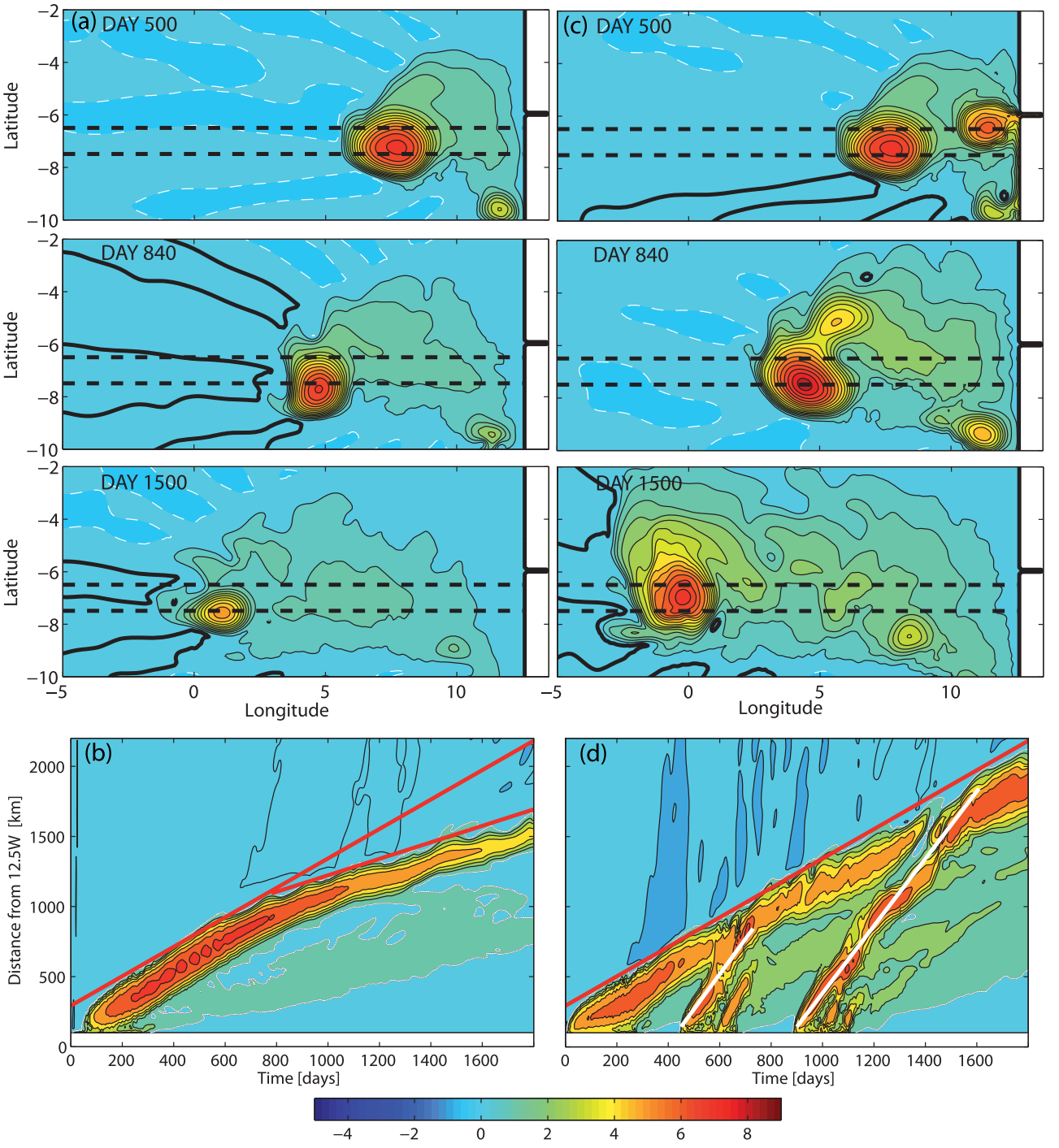

Figure 6. Snapshots of SSH and Hovmöller of SSH from the (left) BSTOP1 and (right) BSTOP2 experiments. CI = 0.5 cm, the black dashed lines in Figures 6a and 6b indicate the 6.5°S and 7.5°S latitude lines. The red lines in Figures 6b and 6d indicate the first eddy (frontal) speed and the white lines in Figure 6d indicate the speed of the trailing eddies.

discharge at selected time intervals. After the formation of the first eddy, we turn off the discharge like in BSTOP1. After this eddy moves away from the river mouth, we turn on the discharge, thus allowing the formation of a second eddy. The procedure is repeated to generate a controlled sequence of three eddies. At day 500, the first bulge eddy is close to 7.5°E and a second eddy starts to develop near the inlet (Figure 6c, top). At day 800, the second eddy catches up and fusioned with the leading one, strengthening the SSH front. Small remnants of the second eddy linger in the northeast region (Figure 6c, middle) but are absorbed later. The snapshot at day 1500 shows that the third eddy (detached from the inlet at day 900)

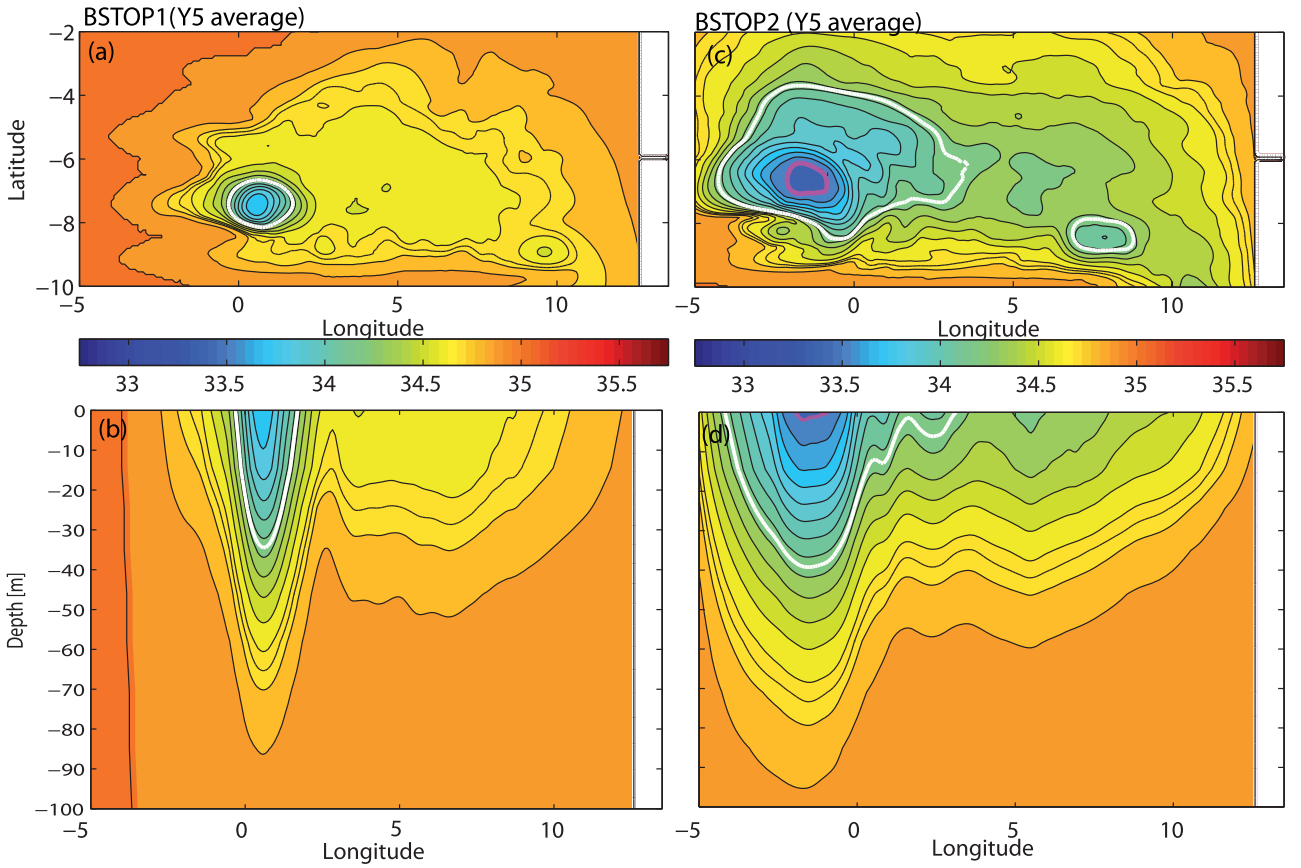

Figure 7. (top) Year averaged SSS and (bottom) cross section of salinity at 6°S from the (left) BSTOP1 and (right) BSTOP2 experiments. CI = 0.1. The magenta and white lines indicate the 33.5 and 34.25 isohalines, respectively.

has already meet and merge with the frontal eddy (Figure 6c, bottom) further enhancing the SSH front. Hövmöller diagrams of the two experiments show that eddy merging sustains not only the strength of the plume's front but also its propagation speed (Figures 6b and 6d). In BSTOP2, there is no secondary's eddy merging. The fusion of the smaller eddies with the slower and bigger bulge eddy has a dominant control on the subsequent structure of the time-averaged plume. At difference with BSTOP1, in BSTOP2, there is a discernable low-salinity pool that covers a large part of the computational domain and with a substantial vertical stratification extending for more than 30 m in the vertical (Figures 7c and 7d).

3.5. Freshwater Balance

NPS02 argued that in near equatorial regions most of the discharge (∼87%) should be funneled toward the coastal current. In our experiments, however, eddies transport a substantial portion of the freshwater discharge into the deep ocean. In fact, the freshwater balance of BENCH shows that, during the first 3 years of model simulation, the coastal current transports only ∼25% of the discharge (Figure 2b). This relatively small freshwater transport is persistently weakened by Rossby wave radiation (Figure 3a) so that in longer integrations most of the freshwater is detrained offshore (Figures 2b and 3b). As we shall show in experiments in stratified basins, the complete dominance of the offshore detrainment occurs more rapidly. This phenomenon is the single most important difference between low-latitude and mid-latitude freshwater discharges.

3.6. Simplified Theoretical Analysis

A near equatorial discharge generates a complex eddy field that diverts most of the freshwater outflow into the deep ocean. In spite of the complexity of the spin-up process, it is possible to rationalize the long-term residual effect of the passage of these eddies without having to consider their complex nonlinear interactions. In other words, it is possible to explain Figure 3b without delving into the details of Figure 3a. To that

end, we assume that the large-scale structure of a NERP is controlled by the linear, reduced-gravity shallow water equations where the dynamical contribution of mesoscale eddies is accounted by Rossby wave dynamics and an eddy diffusion term. If η is the interface displacement, the leading terms of the potential vorticity equation of this system are

$$\frac{\partial}{\partial t}\left[\left(\nabla^2-\frac{1}{R_d^2}-\frac{1}{g'H}\frac{\partial^2}{\partial t^2}\right)\eta\right]+\beta\frac{\partial \eta}{\partial x}=Q'+\Im, \tag{2}$$

where Q' is a point vorticity source representing the near equatorial discharge, H is the mean depth of the fluid, R_d is the Rossby deformation radius $=\sqrt{g'H}/f$, $g'=g\Delta\rho/\rho_o$ is the reduced gravity, $\Im$ represents eddy mixing effects, and ∇ is the horizontal Laplacian. The character of the solutions to equation (2) depend on the time scale considered. At the initial stages, $T_K<1/f$, there are no pressure gradients, therefore, $\frac{\partial \eta}{\partial x}=0$ and equation (2) has Poincaré and Kelvin wave solutions. The former radiate toward the open ocean leaving no residual effect while the later propagate poleward along the continental boundary generating a barotropic pressure gradient that advects the salinity anomaly along the coast [*Matano and Palma*, 2010]. Nonlinear effects [not included in equation (2)] lead to the formation of a growing bulge at the river mouth, which after a time $T_R\sim(\beta L)^{-1}$, starts to radiate offshore as Rossby waves. For $T\gg T_R$, the term $\frac{\partial^2\eta}{\partial t^2}$ is very small compared with the rest of the terms and equation (2) reduces to

$$\frac{\partial}{\partial t}\left[\left(\nabla^2-\frac{1}{R_d^2}\right)\eta\right]+\beta\frac{\partial \eta}{\partial x}=Q'+\Im. \tag{3}$$

If Q' is constant, the steady state version of equation (3) can be transformed into a Helmholtz equation and solved exactly. Its solution, which is the Green's function of the Stommel problem, is called the β-plume and it has been described in some detail by *Vallis* [2006].

In summary, a near equatorial vorticity source at the eastern boundary—like the Congo River discharge—generates a β-plume, and a coastal current, which, in contrast with the midlatitude counterpart, is very weak on account of being subject to enhanced Rossby wave radiation (Figure 8). The partitioning of the discharge between the β-plume and the coastal current depends on the characteristics of the vorticity forcing and the background conditions. Consider, for example, a barotropic discharge, that is a discharge with the same density than the background. In this case, Rossby waves have group velocities,

$$C_g^x=\frac{-\beta\left(-k^2+\frac{1}{R_d^2}\right)}{\left[k^2+\frac{1}{R_d^2}\right]^2}. \tag{4}$$

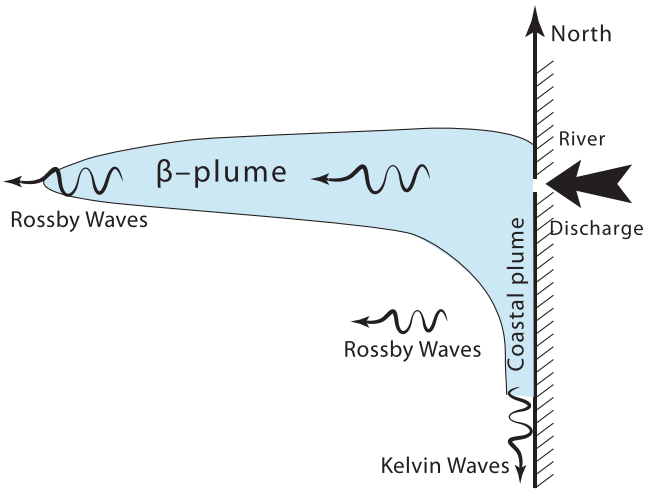

Figure 8. Cartoon showing the long-term time-averaged spatial structure of the SSS field generated by a near equatorial river discharge.

At the beginning of the discharge ($T\sim T_K$), the ocean adjustment is associated with the poleward propagation of Kelvin waves and the establishment of a geostrophically balanced current. For long time scales ($T>T_\beta$), the adjustment proceeds through the generation of barotropic Rossby waves. Since, at low latitudes, R_d is of the order of thousand kilometers $k\gg 1/R_d$ (short waves) and the zonal group velocity reduces to

$$C_g^x=\frac{\beta}{k^2}. \tag{5}$$

Thus, energy will propagate *eastward* and, therefore, most of the river discharge will be funneled toward the coastal current. To illustrate these

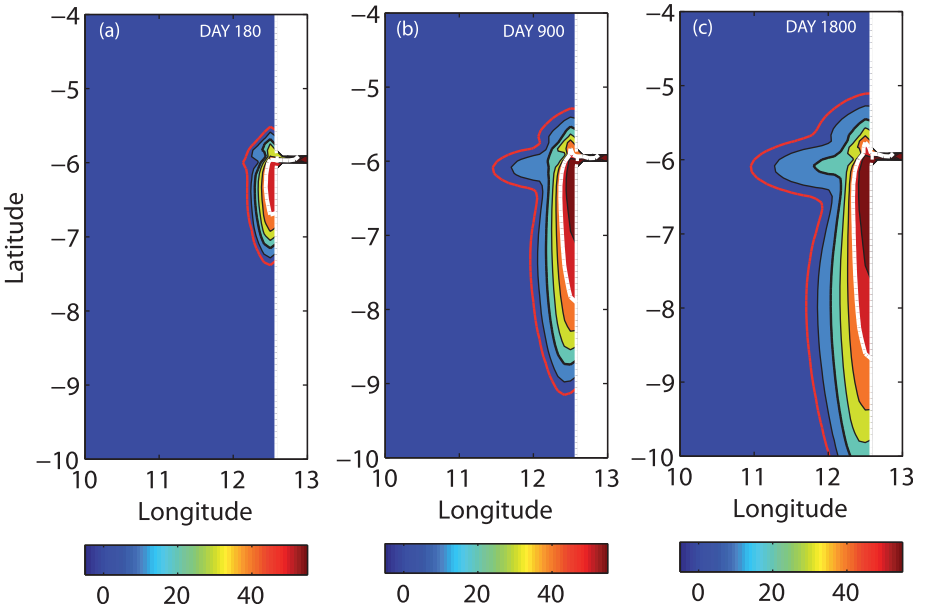

Figure 9. Snapshots of the surface tracer concentration (%) from a barotropic experiment (BBART). CI: 10. The white, black, and red lines indicates the 50, 20, and 5 isolines, respectively.

arguments, we run a barotropic experiment with the same domain as the benchmark but with a discharge of the same salinity as the open ocean (BBART). To track the plume evolution, we continuously release a passive tracer at the mouth of the estuary. As predicted by the above arguments, at short time scales the tracer is advected southward along the coast by the geostrophic currents generated by the Kelvin wave propagation (Figure 9a). At long time scales, the situation does not change substantially except for the formation of a small protuberance near the inlet facing west (Figure 9b). This small "β-plume" grows very slowly with time (Figure 9c). The limited westward migration of the barotropic β-plume compared with the baroclinic case can be explained by the wave dynamics near the inlet. The energy of short Rossby waves produced at $T > T_\beta$ propagates eastward. Upon reaching the coast, most of this energy leaks southward as Kelvin waves. A smaller portion of the incoming energy flux reflects westward as long Rossby waves. This experiment, therefore, shows that the properties of the plume depend on the density difference between the discharge and the ambient waters and, therefore, on the processes regulating these differences within the estuary.

In the baroclinic case, for short time scales ($T \sim T_K$), the ocean adjustment to the initial perturbation is very similar to the barotropic case, the generation of Kelvin waves and the establishment of a coastal current. For long time scales ($T > T_\beta$), the adjustment proceeds again trough the generation of Rossby waves but now the solution changes drastically. The baroclinic R_d is of the order of tens of kilometers, the dynamically important waves will have zonal wavenumbers $k \ll R_d$ (long waves) and the zonal group velocity is now:

$$C_g^x = -\beta R_d^2. \tag{6}$$

That is, energy propagates westward and the perturbation spreads into the ocean interior as the β-plume of BENCH (Figure 3b).

4. Sensitivity Experiments

We did a suite of experiments to assess the sensitivity of BENCH to variations of the outflow characteristics (salinity anomaly and volume magnitude) and the ambient conditions (latitudinal location of the inlet, bottom topography, coastline configuration, and background stratification).

4.1. Outflow Characteristics

For a given geometry of the inlet, i.e., width (W), height (h_i), and latitudinal location, the physical characteristics of the plume depend on the magnitude of the volume flux (Q) and the salinity anomaly (ΔS) of the

discharge. These quantities are connected through the so-called freshwater flux, which is a measure of the freshwater content of the outflow [*Fong and Geyer*, 2002]:

$$Q_{fw} = \frac{Q\Delta S}{S_o}, \tag{7}$$

where S_o is a reference salinity. To assess the sensitivity of BENCH to Q and ΔS, we did two sets of experiments. In the first set of experiments, we kept Q_{fw} fixed and varied Q and ΔS. A wide range of Q and ΔS were examined. We discuss two extreme cases: HDLS (High Discharge Low Salinity), whose volume flux is 4 times larger than BENCH and its salinity anomaly is 4 times lower, and LDHS (Low Discharge High Salinity), whose volume flux is 2 times lower than BENCH and its salinity anomaly is 2 times higher. Both experiments are started from rest and integrated for 16 years.

The largest differences between the HDLS, LDHS, and BENCH are observed near the inlet, where HDLS shows smaller SSS anomalies than LDHS (Figure 10). The eddy train drifts toward the northwest in LDHS and it is more zonal in HDLS. Aside from this, there are no other substantial differences between BENCH and HDLS and LDHS (Figure 10, magenta line). The similarity between BENCH and LDHS is particularly clear. HDLS shows smaller and narrower salinity anomalies near the inlet, which is understandable given its small ΔS yet, in spite of having a huge volume discharge, it shows a spatial structure that is similar to the other

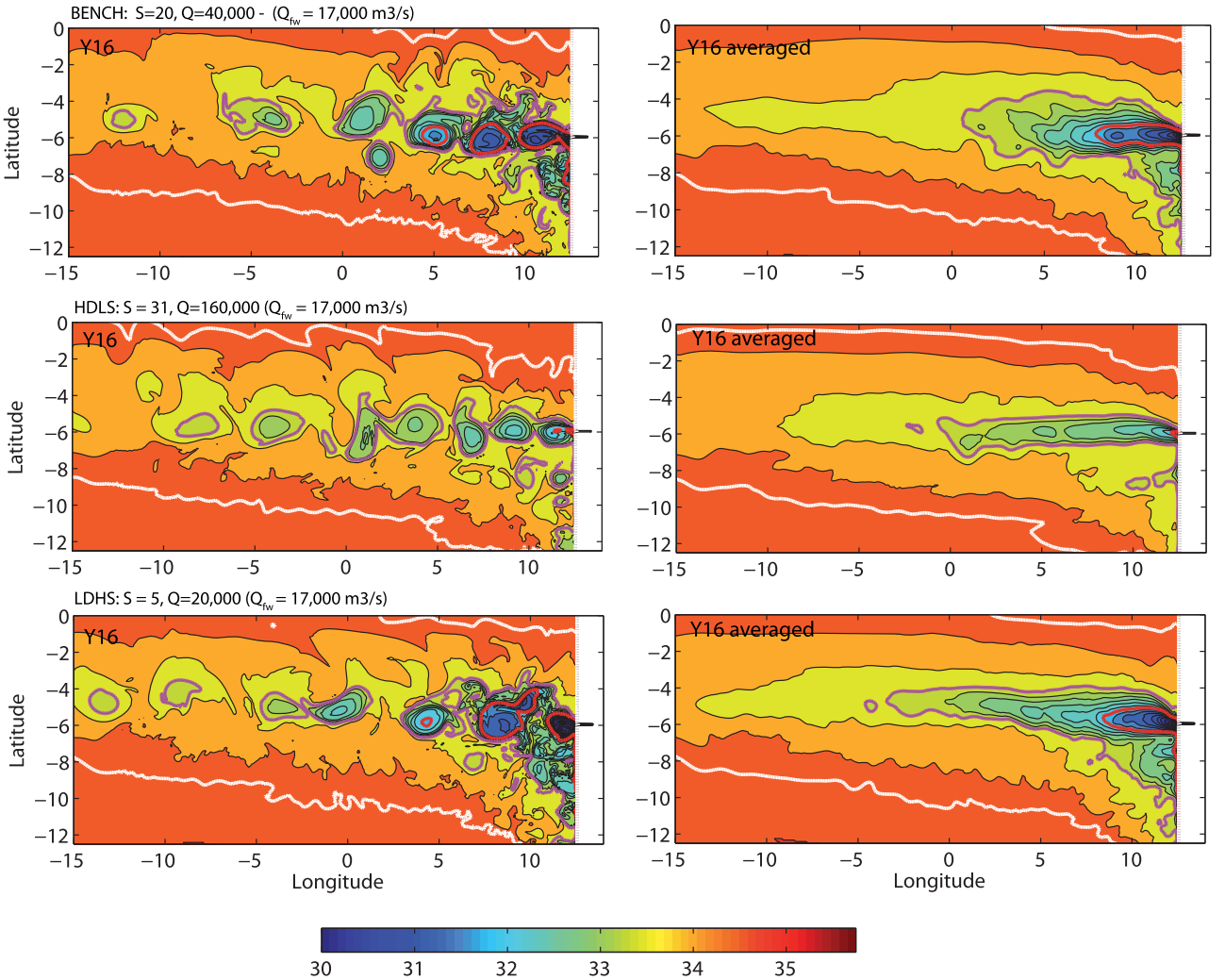

Figure 10. Sea surface salinity from the sensitivity experiments using the same Q_{fw}. (left) Snapshots at the end of year 16 of the simulation. (right) Time-averaged of the last year of integration. (top) From BENCH, (middle) from HDLS, and (bottom) from LDHS. CI and line colors as in Figure 3.

two experiments. The similarity among the three experiments indicates that—away from the inlet region—the large-scale structure of the NERP is more dependent on Q_{fw} than on the particular values of Q and ΔS. In addition, the two sensitivity experiments have westward spreading rates and vertical salinity structures that are nearly identical to the benchmark case (not shown).

The second set of experiments probes the sensitivity of the plume to Q_{fw}. Here we vary Q_{fw} through changes of the Q while maintaining ΔS fixed as in BENCH. This is equivalent to varying the inlet Rossby number $R_{oi} = Q/fh_iW^2$. The salinity anomaly—and therefore the inlet Burger number $B_{ui} = \sqrt{g'H}/fW$—is kept as in BENCH (Table 1). Figure 11 shows a snapshot and the averaged sea surface salinity at year 16 for two extreme cases: LQFW, which has a Q_{fw} that is 4 times smaller than the benchmark, and HQFW, which has a Q_{fw} that is 4 times larger. LQFW produces eddies with a smaller salinity anomaly and a more

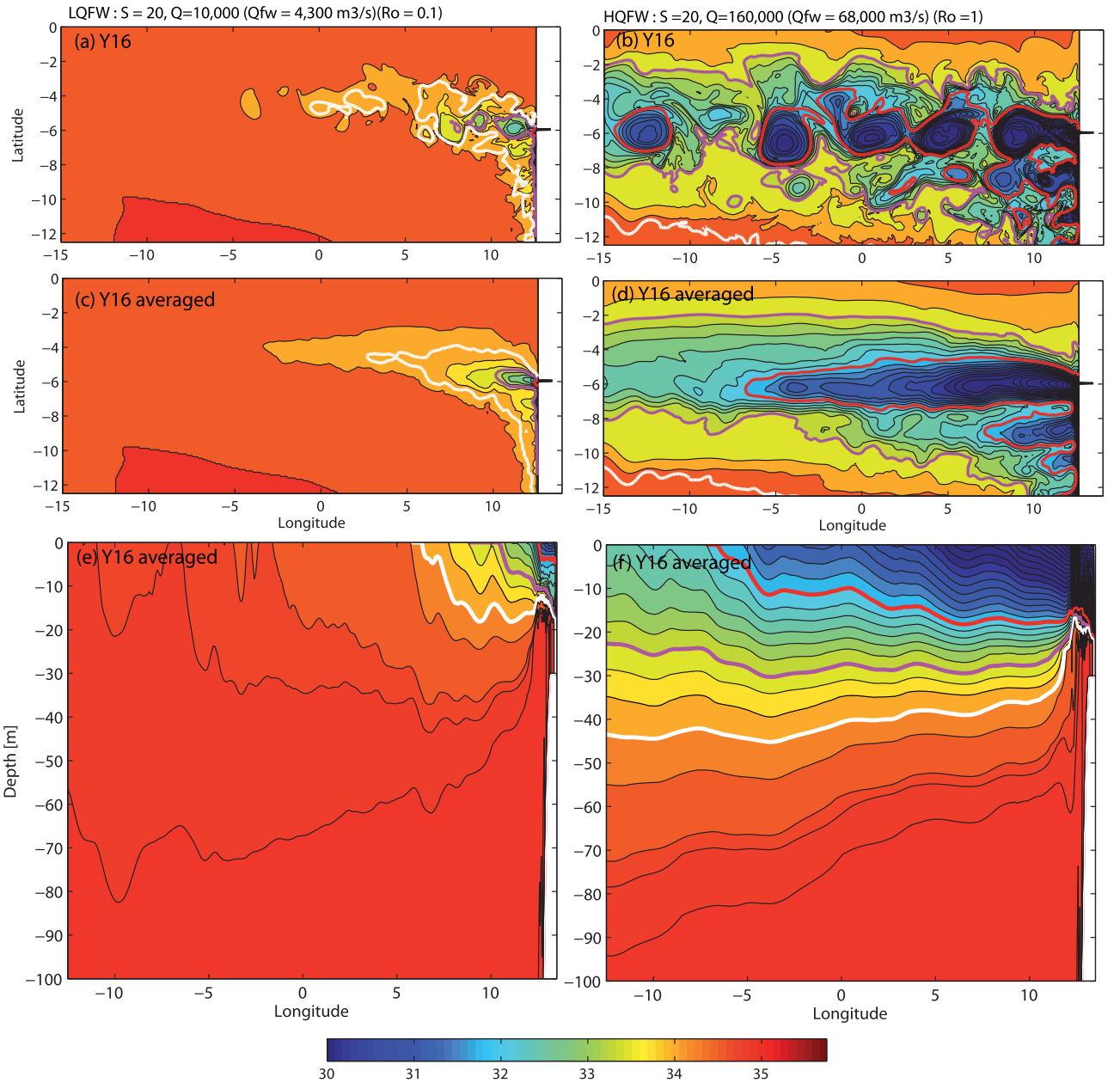

Figure 11. Sea surface salinity and salinity cross sections from the sensitivity experiments varying Q_{fw}. (top) Snapshots at the end of year 16 of the simulation. (middle) Time-averaged results of the last year of simulation. (bottom) Cross sections at 6S. (left) From LQFW (low Q_{fw}) and (right) from HQFW (large Q_{fw}). CI and line colors as in Figure 3.

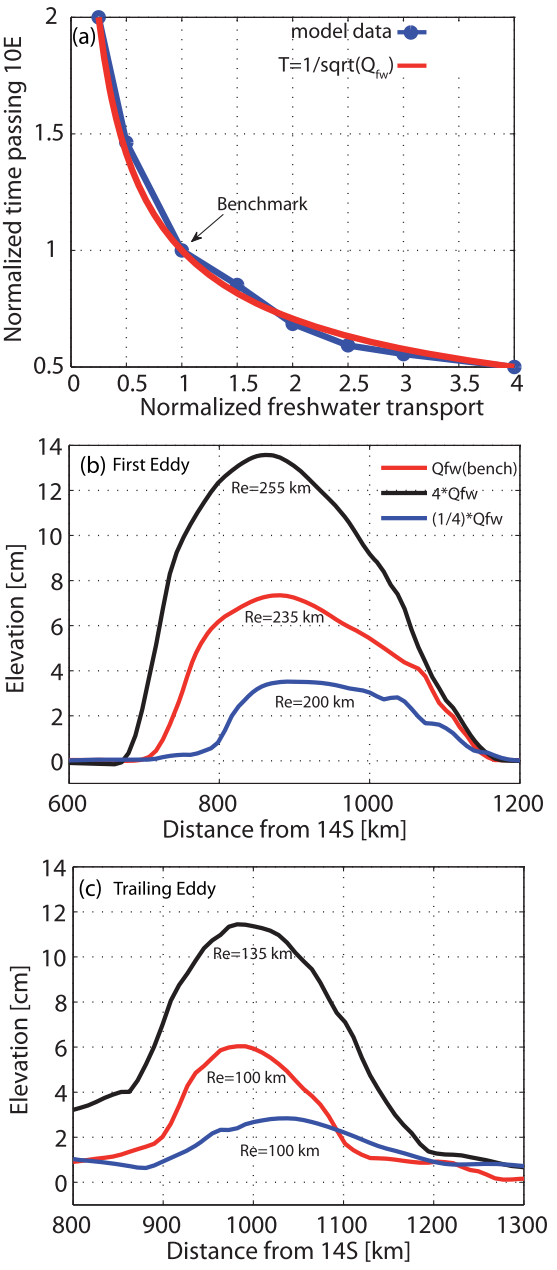

Figure 12. (a) Period of detachment as a function of normalized Q_{fw}. Blue dots indicate the results of different experiments varying Q_{fw}. The red line is an analytical fitting to the experimental values. (b) The size of the first eddy for different values of Q_{fw} computed using SSH. (c) Same as Figure 12b but for the trailing eddies.

northwestward trajectory than BENCH (Figure 11a). HQFW, however, produces larger eddies (size and ΔS amplitude) that spread in a more zonal direction (Figure 11b). The different eddies characteristics of LQFW and HQFW are reflected in their respective plumes (white contours). The LQFW plume, for example, reaches only to 3° while the HQFW spreads beyond the eastern boundary of the model. A noticeable difference between experiments is the appearance of secondary β-plumes in HQFW (Figure 11d), which are drawn from the coastal current. There is a marked reduction of the zonal extent of the plumes, which is partly associated with the weakening of the coastal current and with the increase of latitude (and hence the decrease of the β-effect). The zonal extent of the secondary plumes is also reduced due to eddy dispersion by wave radiation and mixing. Q_{fw} changes also impact in the vertical structure of the plumes. In LQFW, for example, the salinity anomaly extends ∼6° west from the inlet and 15 m in the vertical while in HQFW it extends beyond the eastern boundary of the model and 45 m in the vertical (white line in Figure 11, bottom).

The kinematic characteristics of the eddy field, i.e., horizontal and vertical scale, translation speed, and spreading rate of the plume depend on Q_{fw} or, alternatively, the inlet Rossby number (R_{oi}). HQFW, for example, nearly doubles the spreading rate of BENCH while LQFW spreading rate is nearly half. To quantify the relation between Q_{fw} and the spreading rate, we plotted the period of detachment (see section 3.2) of the first eddy as a function of Q_{fw} (alternatively R_{oi}) for all the experiments listed in Table 1 (Figure 12a). Since the distance between the inlet and 10°E is fixed the passing time reflects the average spreading rate of the salinity front. Our calculation shows that the spreading rate is proportional to the square root of the normalized (by its BENCH magnitude) Q_{fw} (Figure 12a). Fixing Q and varying ΔS, i.e., varying the inlet Burger number (B_{ui}), produce similar results, thus confirming that the kinematic characteristics of NERP eddies are controlled by Q_{fw}. The main difference among eddies in the sensitivity experiments is the magnitude of their SSH anomalies, which increases with Q_{fw} for both the bulge and the trailing eddies (Figures 12b and 12c). The number of trailing eddies passing 10°E is larger for larger Q_{fw} (not shown). The first eddy of LQFW is slower than BENCH thus allowing more interaction with the secondary eddies. This interaction produces a more corrugated SSS field in LQFW (Figure 11a).

Our experiments show that the formation of an eastern boundary NERP is associated with the westward propagation of a train of eddies which lead to the formation of a β-plume. Sensitivity experiments also show that for long time scales (>6 years), this result is independent of the value of Q_{fw} (Figure 11). The

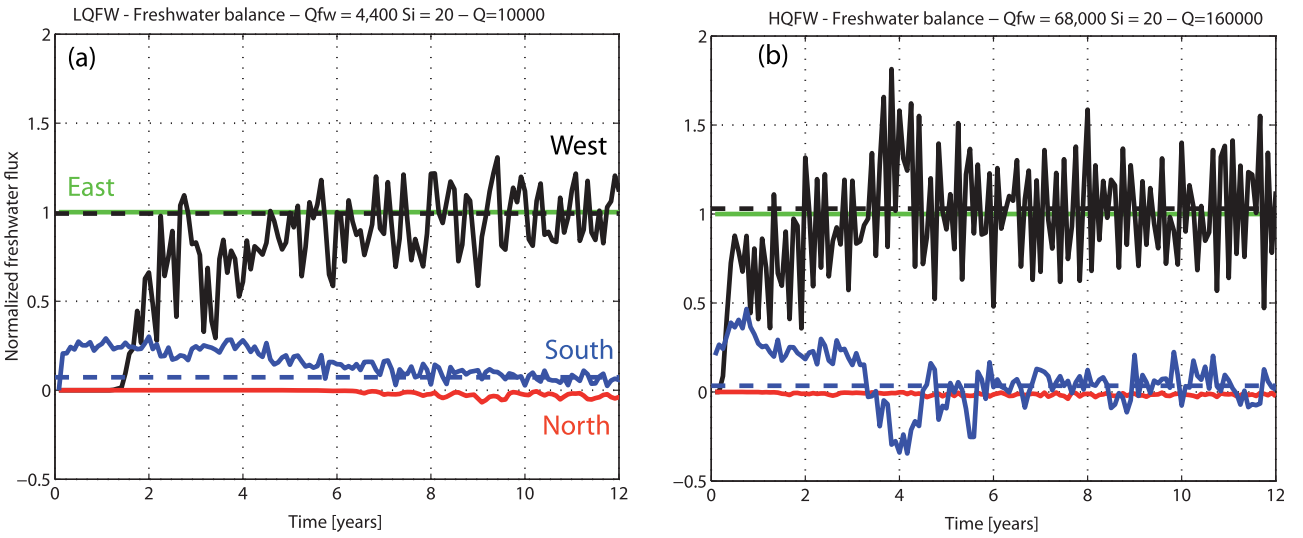

Figure 13. Time evolution of the normalized freshwater transport through the walls of the box indicated in Figure 3a for the experiments (a) LQFW (low Q_{fw}) and (b) HQFW (large Q_{fw}).

time evolution of the freshwater balance, however, depends on Q_{fw}. To facilitate the comparison, the freshwater fluxes depicted in Figure 13 are normalized by the freshwater content of the discharge in each experiment. For low freshwater discharges (LQFW), the coastal current transport remains at ∼0.3 Q_{fw} but persist longer than in the benchmark simulation (Figure 13a). For high freshwater discharges (HQFW), more freshwater is channeled to the coastal current in the first year of simulation although it weakens more abruptly and early compared with the benchmark (Figure 13b). With large inflows, both the coastal current intensity and buoyancy anomaly increase and therefore it is more prone to the development of meanders and eddies through baroclinic instability. After formation, the eddies drift westward and the current intensity and its associated southward transport diminish rapidly. With low discharges, the current is less intense and more stable, sustaining the poleward transport for longer time periods.

4.2. Location of the Discharge

The singular characteristics of NERPs are partly due to the high magnitude of the discharges used in previous experiments but, mostly, to their geographical location. A midlatitude freshwater discharge does not form a train of westward propagating eddies but a growing bulge and a coastal current (VIC14).

To further demonstrate the importance of the β-pulling effect on the development of NERPs, we did two additional experiments: one in which the inlet is located at 3°S, thus increasing the β-pulling effect (LAT3E) and the other keeping the inlet at its original latitude but moving it to the western boundary (LAT6W). Moving the inlet to 3°S leads to larger and faster eddies that disperse more rapidly (Figure 14, middle). Due to the strengthening of the β-effect, the NERP eddies lose rapidly their circular symmetry becoming more zonally elongated (Figure 14c). The rapid propagation of these eddies erodes the freshwater signature of the discharge near the inlet, which is noticeably weaker than at 6°S (Figure 14, top). The overall effect of the latitudinal change is clearly reflected in the time-averaged plume (Figure 14d), which is more zonal than BENCH and extends farther west. In fact, at year 3, the LAT3E plume already extends to the western boundary of the model, while the BENCH plume has only reached to 0°E. The increase of the β-effect in LAT3E affects the partition between the β-plume and the coastal current, which translates into a strengthening of the former and a weakening of the later.

LAT6W shows quite different plume characteristics (Figure 14e). The initial adjustment of this experiment resembles the midlatitude case where, after debouching into the ocean, the plume moves alongshore in the direction of the coastally trapped waves [e.g., *Nof and Pichevin*, 1999]. However, after reaching the equatorial region, the plume is advected eastward by the quasi-geostrophic currents generated by the propagation of equatorial Kelvin waves. The plume evolution is faster than in LAT3E on account of the fact that the adjustment is associated with Kelvin instead of Rossby wave propagation. By year 3, for example, the plume

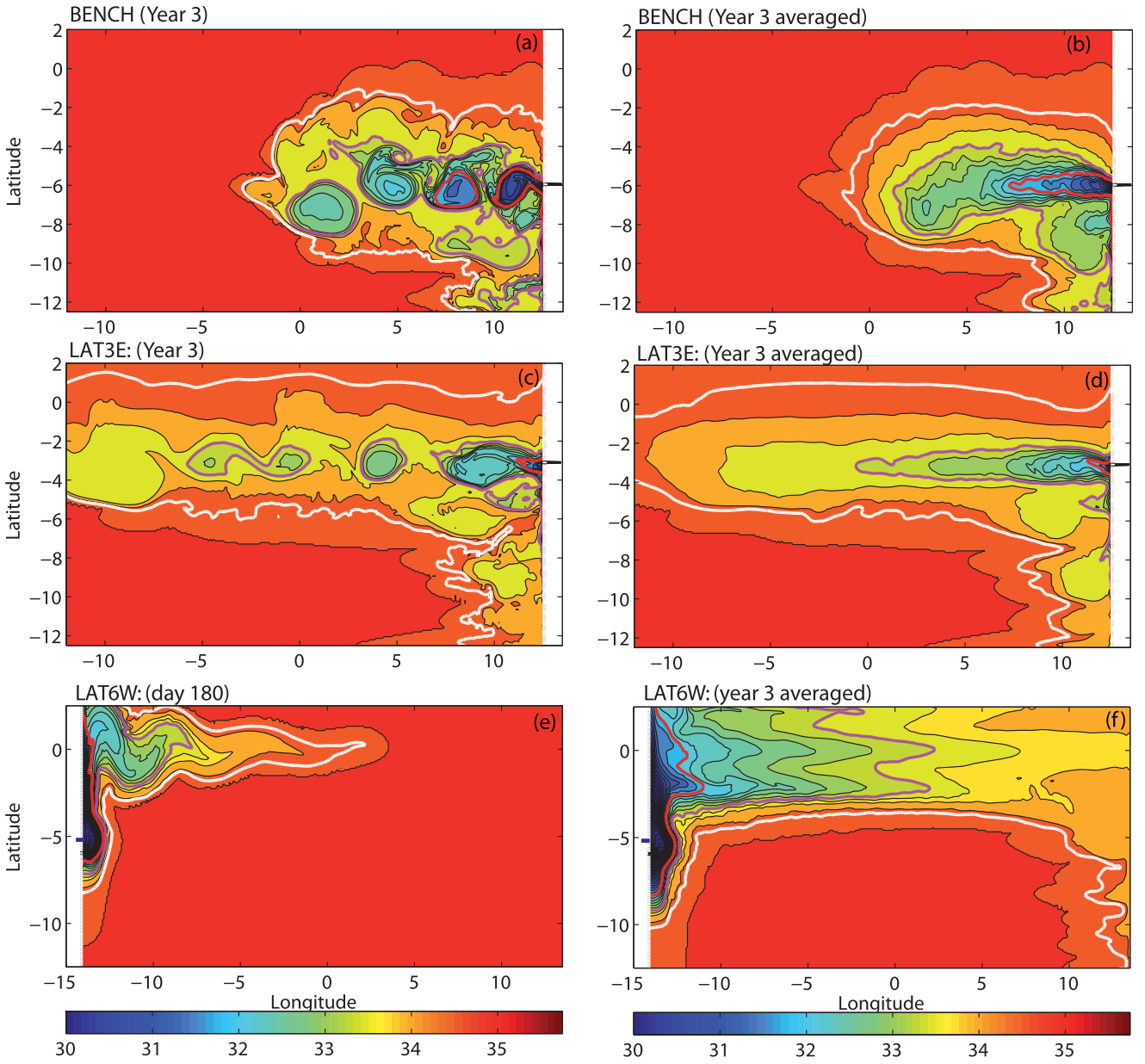

Figure 14. Sea surface salinity from the sensitivity experiments varying the location of the inlet. (left) Snapshots at specific times. (right) Time-averaged results of the last year of simulation (year 3). (top) From BENCH, (middle) from LAT3E, and (bottom) from LAT6W. CI and line colors as in Figure 3.

of LAT6W has not only reached the eastern boundary but also spread toward the midlatitude regions of both hemispheres (Figure 14f).

4.3. Bottom Topography

At difference with our benchmark experiment, which has a constant depth of $H = 1000$, NERPs usually debouches into continental shelves of varying dimensions. To explore the impact of the bottom topography on the characteristics of NERP's eddies, we did three additional experiments varying the bottom topography: SHELFN has a narrow shelf ($\sim$65 km, like the Congo River) [*Saboye et al.*, 2009], SHELFW has a wide shelf (400 km), and HCONST has a shallower (constant) depth (50 m). The results of SHELFN are similar to those of BENCH (Figures 15a and 15b). There is, however, a small meridional shift of the eddy corridor and of the plume axis toward 5°S. When the shelf has a gentle slope, the growing and deepening bulge feels the bottom and the eddy trajectories are deflected northward (Figure 15c). Once there, the larger β-pulling forces and faster Rossby waves lead to a zonal elongation and more rapid propagation of the eddies

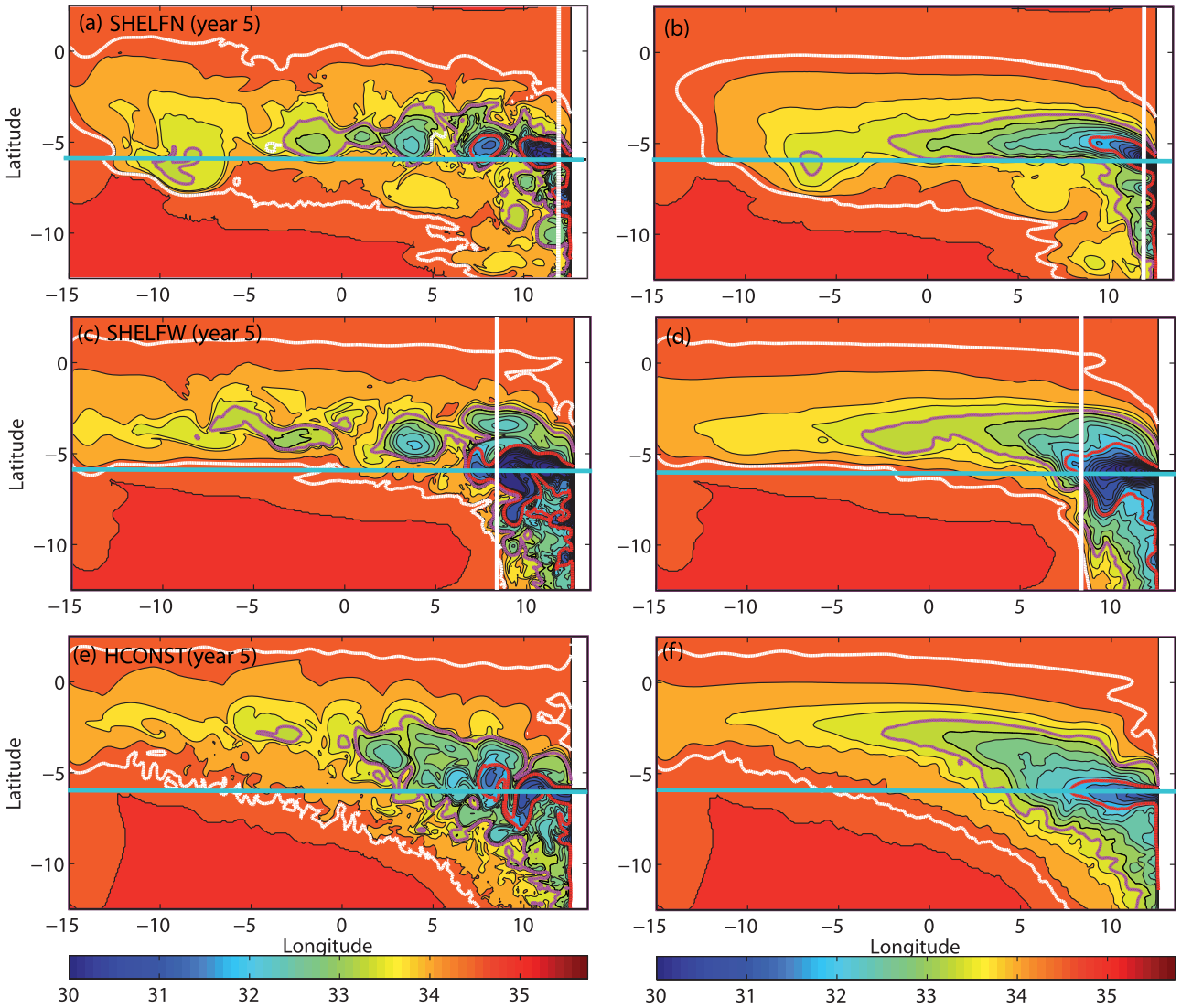

Figure 15. Sea surface salinity from the sensitivity experiments varying the bottom topography. (left) Snapshots at the end of year 5. (right) Time-averaged results of the last year of simulation. (top) From SHELFN (narrow shelf), (middle) from SHELFW (wide shelf), and (bottom) from HCONST (constant bathymetry). The white meridional line in the top and middle indicate the shelf break. The cyan line indicates the latitude of the inlet. CI and line colors as in Figure 3.

(Figure 15c). The final result is a wider near-field plume covering almost the entire shelf and an offshore plume with an axis displaced northward, toward 3.5°S (Figure 15d).

Cushman-Roisin [1994] explained the northward displacement of an anticyclonic eddy with the center of mass initially moving westward toward deeper waters. Consider a fluid column on the northern and southern flanks of the first eddy. The advection of surrounding fluid induces, after a quarter turn, an anticyclonic vortex (via vortex stretching) on the western side of the eddy and a corresponding cyclonic vortex (via vortex squeezing) on the eastern side. The cumulative effect is a slow migration of anticyclonic eddies toward the north. It is interesting to note that, as long as the first eddy isohalines touch the bottom at some instant, it is not necessary to have a bottom gradient to induce this secondary movement. In an experiment with constant bottom (HCONST) after the first eddy is big enough to feel the bottom, their own core fluid undergoes a similar squeezing mechanism and a consequent northward movement to conserve potential vorticity (Figures 15e and 15f).

4.4. Coastline Configuration

VIC14 argued that the slant of the African coast produces a northward shift and degradation of the eddy train generated by the Congo River discharge. It seems reasonable to surmise, therefore, that plumes

emanating from a slanted coastline will differ from those emanating from a meridional coastline since the momentum balance of the plume depends on the along-wall component of the discharge (NPS02). To address these matters, we did two additional experiments maintaining the direction of the discharge (or the estuary) but varying the inclination of the coastal boundary. In SLNE, the discharge is slanted toward the northeast and in SLNW the discharge is slanted toward the northwest.

The coastal inclination affects the shape of the plume. Comparison between BENCH and SLNE shows a northward shift of the plume axis, which reflects a similar shift of the eddy train, and a westward reduction of the plume's fetch (Figure 16a). The larger freshwater pool in the near-field region (east of ~7°W) leads to a larger downstream flow. SLNW, which mimics the inclination of the African coastline, shows opposite characteristics (Figure 16b). To assess the impact of the coastline inclination on the plume characteristics, we consider the steady state, along-wall momentum balance described in NPS02. In this balance, the sum of the "*momentum flux force*" or "*reactive force*" (F_{cc}) associated with the coastal jet and the β-force (F_β) generated by the variation of the Coriolis parameter between the northern and southern sides of the bulge is arrested by the integrated Coriolis force provided by the westward motion of the eddy center of mass (F_c)

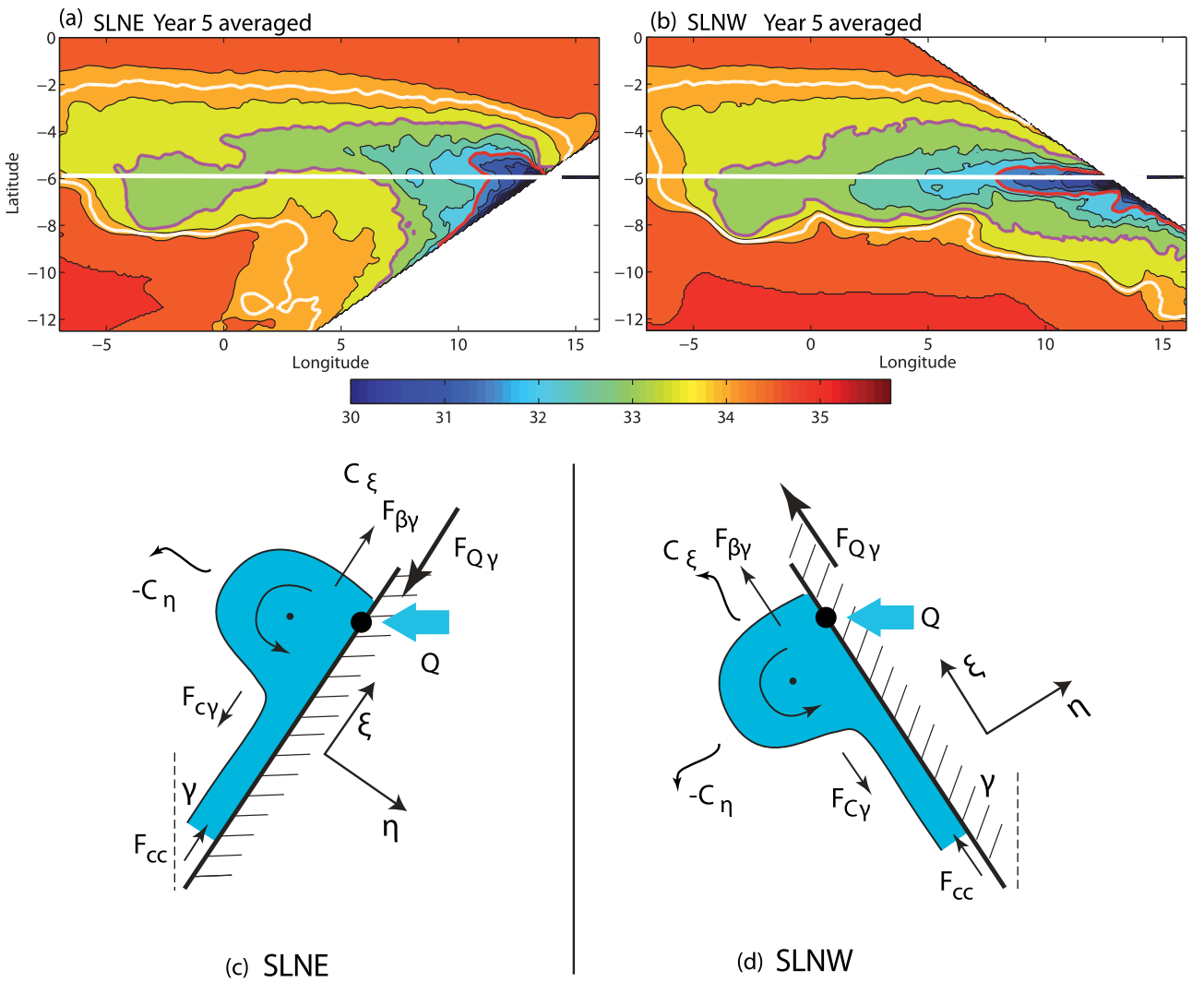

Figure 16. (top) Time-averaged sea surface salinity from the sensitivity experiments varying the coastline orientation. (bottom) Schematic diagrams indicating the balance of the alongshore forces acting in the near field. (left) From experiment SLNE (slanted coast oriented in a NE direction). (right) From SLNW (slanted coast oriented in a NW direction). In Figure 16d, the alongshore Coriolis force $F_{c\gamma}$, resulting from the eddy migration in the offshore direction (C_η) balances the jet force associated with the coastal current F_{cc}, the β induced force $F_{\beta\gamma}$ and the projection of the jet force associated with the outflow ($F_{Q\gamma}$). In Figure 16c, $F_{c\gamma}$ and $F_{Q\gamma}$ balance the sum of the jet force F_{cc} and the β induced force $F_{\beta\gamma}$. These diagrams have been adapted from NPS02.

(NPS02). If the wall is slanted at an angle γ, there is a new force that represents the along-wall "*reactive force*" ($F_{Q\gamma}$) given by the projection of the river discharge onto this direction (Figure 16c). The difference between SLNW and SLNE is that in the latter case $F_{Q\gamma}$ is opposite to F_{cc} and, therefore, a smaller Coriolis force is needed to balance the reactive force of the coastal current (Figure 16c). As a consequence, during the first stages of the experiment (the time taken for the first eddy to detach from the wall), there is an increase of the buoyant flux toward the downstream direction. NPS02 theory assumes steady state and the existence of a well-defined coastal current. As the flow evolves, however, this condition is not strictly fulfilled because instabilities and eddy-shedding reduce the downstream freshwater transport. Nonetheless, the cumulative dynamical effect of the modified momentum balance reduces the westward expansion of the plume and increases the downstream buoyancy flux (Figure 16a). In SLNW, the situation is reversed (Figure 16d). In this case, $F_{Q\gamma}$ acts in the same direction as F_{cc} and the (westward) motion of the eddies must be enhanced to attain a steady state, thus producing a larger westward penetration of the plume (Figure 16b). The difference in westward spreading of the outflow influence among experiments can be quantified in terms of the meridionally averaged freshwater content of the surface layer in the region of the plume's influence. In consonance with the SSS distribution shown in Figures 16a and 16b, the freshwater content is larger for SLNE in the near field (eastward of $\sim$7°W), but it decreases faster than SLNW afterward (not shown), thus corroborating that SLNW has a larger impact on the far field than SLNE. Moreover, the NW component of the inflow in SLNW carried some of the freshwater northward, producing a larger upstream dispersion of the low-salinity anomaly along the coast (the intersection of the white line with the coast in Figures 16a and 16b).

4.5. Ambient Stratification

To assess the impact of background stratification, we did an additional experiment, STRAT, in a vertically stratified basin. In this experiment, the initial density profile is similar to that of the last year of the BENCH experiment. This profile, therefore, represents the background conditions created by the discharge through 16 years of numerical simulation. STRAT has a lower SSS value than BENCH. To facilitate the comparison between these experiments, the salinity distribution of STRAT was offset (at all depths) by a constant value so as to have the same SSS than BENCH. STRAT was started from rest and run for a relatively short (5 year) period to avoid a significant drift of the background conditions.

There are substantial differences between BENCH and STRAT (Figure 17). Most notably, STRAT does not show the eddy merging process that characterized BENCH. Instead, there is regular train of westward directed eddies that—except in the initial stages of the simulation—do not interact with each other (Figure 17b). There is, moreover, no formation of an oversized bulge during the spin-up, which has the approximate size of the subsequent eddies. STRAT eddies move faster than the bulge eddy of BENCH and therefore its SSS front advances more rapidly. STRAT eddies, for example, cross the basin in 2.7 years while in BENCH the bulge eddy takes 7 years (Figure 17a, year 5). STRAT eddies are smaller and faster than the bulge eddy of BENCH but are comparable in size and speed to the secondary eddies. The contribution of eddy merging is also appreciated in the SSS averages, which show that the salinity plume of STRAT has not only a smaller amplitude but also a more reduced spatial coverage, in spite of the fact that the STRAT eddies move faster than those of BENCH (Figures 17c and 17d).

One of the most important differences between BENCH and STRAT is that the later shows the development of a vigorous cyclonic eddy field. In a stratified fluid, the shedding of anticyclones provides a negative potential vorticity source for the formation of cyclones. After formation, cyclones and anticyclones form dipole structures characterized by the dominance of the later. Cyclones, nevertheless, play an important role in the structure of the NERP. Their westward progression lowers the SSH level of the northern portion of the domain shifting the zero SSH contour and thus arresting the northern penetration of the NERP (Figure 18a). The upwelling generated by the cyclones, moreover, pumps saltier water to the surface (Figures 18b and 18c) thus reducing the SSS anomaly generated by the freshwater discharge (Figure 17d). Cyclonic upwelling, in fact, is more important to the long-term structure of the NERP than the eddy merging effect, which is restricted to the initial phases of the plume evolution.

In summary, the two most important changes brought by STRAT are a change of the characteristics of the eddies, which are smaller, move faster and have more infrequent interactions with each other and the

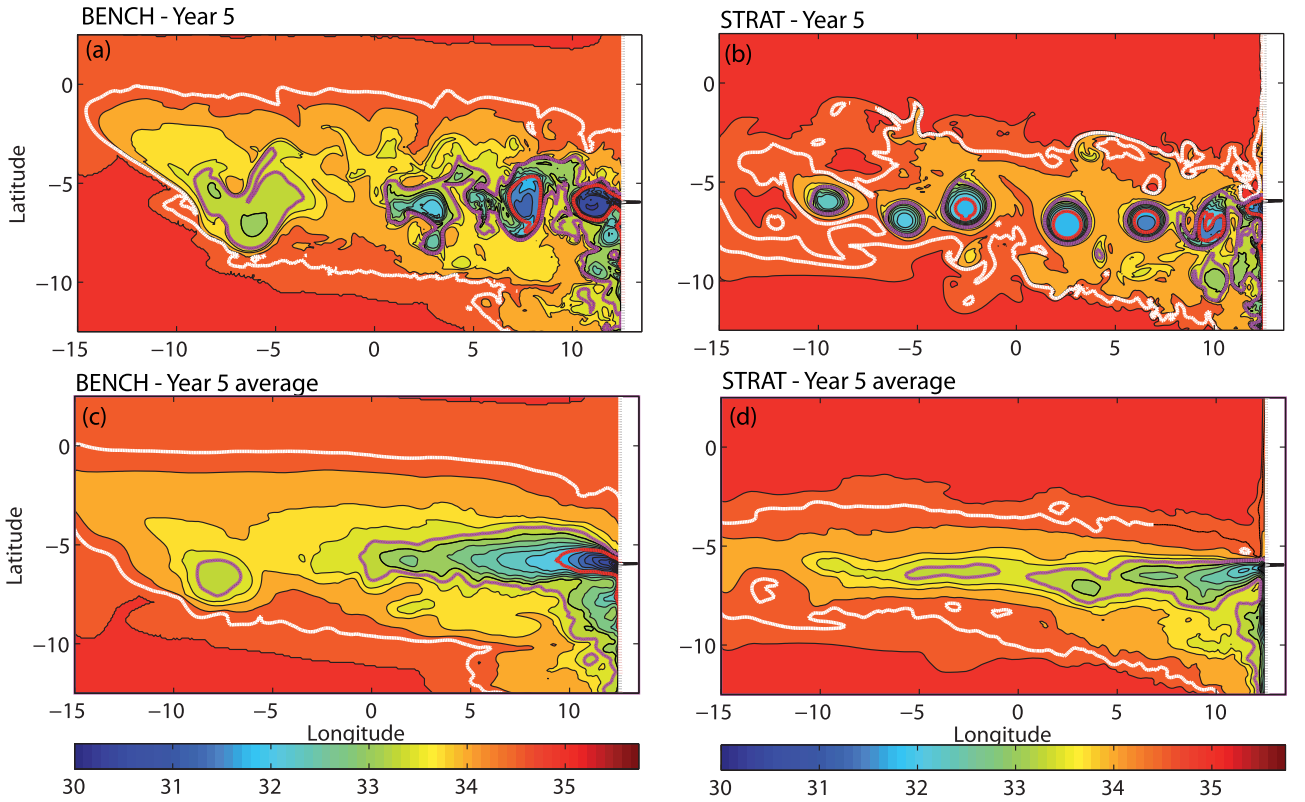

Figure 17. Sea surface salinity from the sensitivity experiments varying the initial stratification. (top) Snapshots at the end of year 5. (bottom) Time-averaged results of the last year of simulation. (left) From BENCH (uniform initial conditions) and (right) from STRAT (vertically stratified initial conditions). CI and line colors as in Figure 3.

emergence of a vigorous field of cyclones, which cause a significant decrease of the SSS anomaly and the northward extent of the NERP. It is obvious that long-term integrations of BENCH will produce results similar to those of STRAT. The comparison of the initial phases of both experiments, however, allows to identify dynamically important processes such as the development of a cyclonic eddy field, which contribute to the shaping of the NERP. To the best of our understanding, there are no previous studies on the impact of cyclones on the upper ocean SSS structure.

5. Summary and Conclusions

The oceanic adjustment to a low-latitude freshwater discharge has three well-defined phases. In the initial stages, Kelvin waves propagate the volume anomaly along the continental boundary, thus generating a barotropic pressure gradient and a geostrophic flow that advects the salinity anomaly along the coast [*Matano and Palma*, 2010]. Near the inlet, the discharge leads to the formation of a bulge which grows until the β-effect forces its detachment from the coast (NPS02). The detachment of the bulge is followed by a succession of smaller eddies that travel faster, on account of the change of the background conditions created by the propagation of the bulge eddy. The collision between the smaller eddies and the bulge eddy is a distinctive phase of the spin-up that compensates the decay of the salinity anomaly to diffusive processes and generates the background density stratification upon which further eddies evolve. The nonlinear merging of eddies is an important mechanism for the westward spreading and strengthening of the low-salinity front generated by the river discharge. Without it, the eddies would be constantly eroded by Rossby wave radiation and background mixing. One of the most important differences between eastern boundary, low-latitude and midlatitude buoyant plumes is that in the later the freshwater discharge is funneled to the coastal current while in the former the discharge is detrained offshore.

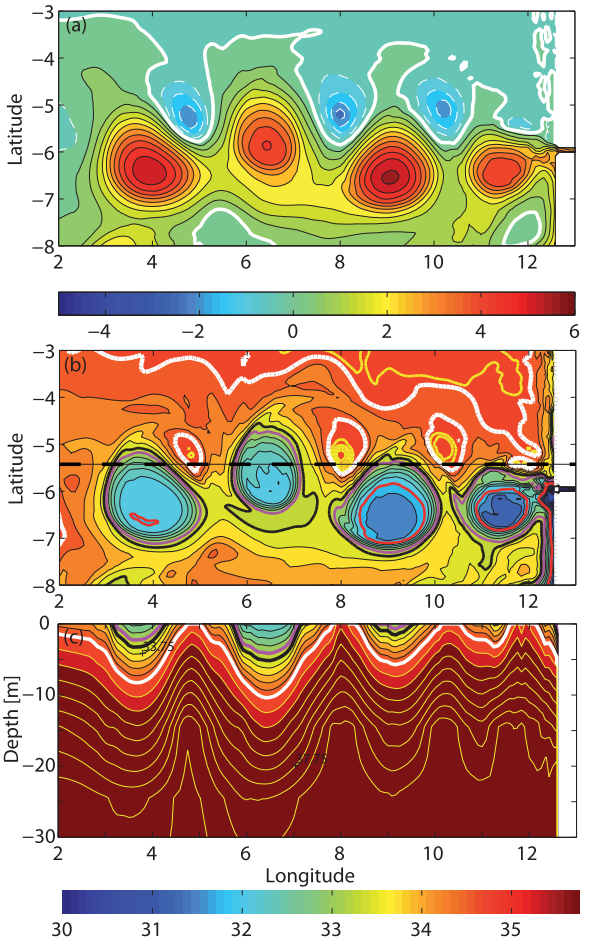

Figure 18. Snapshots of (a) SSH and (b) SSS from the STRAT experiment. (c) Cross section of salinity along the black dashed line indicated in Figure 18b. CI is 0.5 cm for SSH and 0.25 for salinity. The white line is the zero contour for SSH and the 34.75 for SSS. The red, magenta, and black lines indicate the 32, 33.25, and 33.5 isohalines, respectively. The yellow lines indicate salinity contours above 35.

Sensitivity experiments show that the spreading rate and salinity structure of low-latitude plumes are modulated by the magnitude of the freshwater flux (Q_{fw}), the geographical location of the outflow, the inclination of the coast, the depth of the shelf, and the background stratification. Low-latitude plumes, however, appear to be largely insensitive to the individual magnitudes of Q and ΔS as long as they produce similar values of Q_{fw}. We found that larger Q_{fw} generates bigger and well-defined eddies that propagate more zonally with a spreading rate that is proportional to the square root of the normalized Q_{fw}. For the largest value of Q_{fw} tested, the model showed the appearance of secondary β-plumes southward of the inlet produced by the β-pulling of the coastal current waters. The increase in Q_{fw} also impacts on the magnitude of the SSH anomalies for the bulge and the secondary eddies. It is interesting to note that in spite of these differences, the sensitivity experiments demonstrate that for long time scales (>6 years), the bulk of the discharged water spreads westward irrespective of the amount of Q_{fw}.

VIC14 ascribed the equatorward displacement and degradation of the Congo plume in their more realistic experiment to the combination of the β-effect and the local geomorphology. We found that only wide shelves have a sizable influence on the eddy generation because—in this case—the growth and deepening of the bulge can be influenced by vortex stretching effects. Near the equator, the β increases and, therefore, Rossby waves propagate faster. Thus, in a basin with a wide shelf and a gentle bottom slope, eddies are more zonally elongated and disperse faster. A freshwater discharge in a narrow shelf (like the real Congo River shelf), however, should not be significantly different than in the BENCH experiment. We surmise, therefore, that VIC14 results are more related to the slant of the coastline and the shallowing of the inlet than to the shelf bathymetry. Experiment SLNW shows that if the river debouches on an eastward coast slanted in the NW direction, the low-salinity anomaly extends farther equatorward along the coastline than in BENCH. This difference can be attributed to changes in the dynamical balance of the near-field region as compared with a meridional coastline. Moreover, ancillary experiments (not shown) shallowing the inlet (below 30 m) but keeping the same ocean depth as BENCH also exhibit a northwestward spread of the eddy train. Finally, we found that the background stratification, which suppresses the eddy merging process observed in unstratified basins and leads to the formation of a cyclonic eddy field, has a substantial impact on the characteristics of NERPs.

The experiments discussed in this article are a first step in a series of studies that aim to characterize the kinematics and dynamics of particular NERPs (like the Congo River discharge). Further studies in more realistic model setups will discuss the impact of atmospheric forcing and the oceanic mean circulation on NERPs. At this stage, however, the highly idealized configuration of the model precludes direct comparison with observations.

Acknowledgments
E. D. Palma acknowledges the financial support from Agencia Nacional de Promoción Científica y Tecnológica (grant PICT12-0467), Universidad Nacional del Sur (grant 24F044), and MINCyT/CONAE (grant 001), Argentina. R. Matano acknowledges the financial support of NASA through grant NNX08AR40G, NOAA through grant NA13OAR4310132, and the National Science Foundation through grant OCE-1559550. The comments of Ms. Emily Lemagie are kindly appreciated. The paper benefited substantially from suggestions given by the anonymous reviewers. The source code for the model used in this study, ROMS, is freely available at https://www.myroms.org/. Both the data and input files necessary to reproduce the experiments with ROMS are available from the authors upon request (uspalma@criba.edu.ar).

References

Beldamani, A., N. A. Maximanko, J. P. McCreary, R. Furue, O. V. Melnichenko, N. Schneider, and E. Di Lorenzo (2013), Linear wind-forced beta plumes with application to the Hawaiian Lee Countercurrent, *J. Phys. Oceanogr.*, *43*, 2071–2094.

Chao, Y., J. D. Farrara, G. Schumann, K. M. Andreadis, and D. Moller (2015), Sea surface salinity variability in response to the Congo river discharge, *Cont. Shelf Res.*, *99*, 35–45.

Chassignet, E. P., and B. Cushman-Roisin (1991), On the influence of a lower layer on the propagation of nonlinear oceanic eddies, *J. Phys. Oceanogr.*, *21*, 939–957.

Cushman-Roisin, B. (1994), *Introduction to Geophysical Fluid Dynamics*, 317 pp., Prentice Hall, N. J.

Dai, A., T. Qian, K. E. Trenberth, and J. D Milliman (2009), Changes in continental freshwater discharge from 1948–2004, *J. Clim.*, *22*, 2773–2791.

Denamiel, C., W. P. Budgell, and R. Toumi (2013), The Congo River plume: Impact of the forcing on the far-field and near-field dynamics, *J. Geophys. Res. Oceans*, *118*, 964–989, doi:10.1002/jgrc.20062.

Fong, D. A., and W. R. Geyer (2002), The alongshore transport of freshwater in a surface-trapped river plume, *J. Phys. Oceanogr.*, *32*, 957–972.

García Berdeal, I., B. M. Hickey, and M. Kawase (2002), Influence of wind stress and ambient flow on a high discharge river plume, *J. Geophys. Res. Oceans*, *107*(C9), 3130, doi:10.1029/2001JC000932.

Garvine, R. W. (1999), Penetration of buoyant coastal discharge onto the continental shelf: A numerical model experiment, *J. Phys. Oceanogr.*, *29*, 1892–1909.

Hopskins, J., M. Lucas, C. Dufau, M. Sutton, J. Stum, O. Lauret, and C. Channelliere (2013), Detection and variability of the Congo River plume from satellite derived sea surface temperature, salinity, ocean colour and sea level, *Remote Sen. Environ.*, *139*, 365–385.

Marchesiello, P., J. C. McWilliams, and A. Shchepetkin (2001), Open boundary conditions for long-term integration of regional oceanic models, *Ocean Modell.*, *3*, 1–20.

Matano, R. P., and E. D. Palma (2010), The spindown of bottom-trapped plumes, *J. Phys. Oceanogr.*, *40*, 1651–1658.

Materia, S., S. Gualdi, A. Navarra, and L. Terray (2012), The effect of Congo River freshwater discharge on Eastern Equatorial Atlantic climate variability, *Clim. Dyn.*, *39*, 2109–2125.

Nof, D., and T. Pichevin (1999), The establishment of the Tsugaru and the Alboran gyres, *J. Phys. Oceanogr.*, *29*, 39–54.

Nof, D., and T. Pichevin (2001), The ballooning of outflows, *J. Phys. Oceanogr.*, *31*, 3045–3058.

Nof, D., T. Pichevin, and J. Sprintall (2002), Teddies and the origin of the Leeuwin Current, *J. Phys. Oceanogr.*, *32*(9), 2571–2588.

Nof, D., S. Van Gorder, and T. Pichevin (2004), A different outflow length scale?, *J. Phys. Oceanogr.*, *34*(4), 793–804.

Oey, L.-Y., and G. L. Mellor (1993), Subtidal variability of estuarine outflow, plume, and coastal current: A model study, *J. Phys. Oceanogr.*, *23*, 164–171.

Saboye, B., N. Babonneau, B. Dennielou, and M. Bez (2009), Geological overview of the Angola–Congo margin, the Congo deep-sea fan and its submarine valleys, *Deep Sea Res., Part II*, *56*, 2169–2182.

Shchepetkin, A. F., and J. C. McWilliams (2005), The regional oceanic modeling system (ROMS): A split-explicit, free-surface, topography-following-coordinate oceanic model, *Ocean Modell.*, *9*, 347–404.

Smolarkiewicz, P. K., and W. W. Grabowski (1990), The multidimensional positive definite advection transport algorithm: Nonoscillatory option, *J. Comput. Phys.*, *86*, 355–375.

Vallis, G. K. (2006), *Atmospheric and Oceanic Fluid Dynamics; Fundamentals and Large Scale Circulation*, 745 pp., Cambridge Univ. Press, Cambridge, U. K.

Vic, C., H. Berger, A. M. Tréguier, and X. Couvelard (2014), Dynamics of an equatorial river plume: Theory and numerical experiments applied to the Congo plume case, *J. Phys. Oceanogr.*, *44*, 980–994.

Yankovsky, A. E. (2000), The cyclonic turning and propagation of buoyant coastal discharge along the shelf, *J. Mar. Res.*, *58*, 585–607.

Yankovsky, A. E., and D. C. Chapman (1997), A simple theory for the fate of buoyant coastal discharges, *J. Phys. Oceanogr.*, *27*, 1386–1401.